Journal of Experimental Botany
https://doi.org/10.1093/jxb/erae417 Advance Access Publication 9 October 2024

RESEARCH PAPER

Multi-scale phenotyping of senescence-related changes in roots of rapeseed in response to nitrate limitation

Maxence James[1,†], Céline Masclaux-Daubresse[2,†], Thierry Balliau[3], Anne Marmagne[2], Fabien Chardon[2], Jacques Trouverie[1,†], and Philippe Etienne[1,†,*]

[1] Université de Caen Normandie, INRAE, UMR 950 EVA, SFR Normandie Végétal (FED4277), 14000 Caen, France
[2] Université Paris-Saclay, INRAE, AgroParisTech, Institute Jean-Pierre Bourgin for Plant Sciences (IJPB), 78000, Versailles, France
[3] Université Paris-Saclay, INRAE, CNRS, AgroParisTech, UMR GQE-Le Moulon, 91190 Gif-sur-Yvette, France

[†] These authors contributed equally to this work.
* Correspondence: philippe.etienne@unicaen.fr

Received 6 June 2024; Editorial decision 27 September 2024; Accepted 8 October 2024

Editor: Peter Bozhkov, Swedish University of Agricultural Sciences, Sweden

Abstract

Root senescence remains largely unexplored. In this study, the time-course of the morphological, metabolic, and proteomic changes occurring with root aging were investigated, providing a comprehensive picture of the root senescence program. We found novel senescence-related markers for the characterization of the developmental stage of root tissues. The rapeseed root system is unique in that it consists of the taproot and lateral roots. Our study confirmed that the taproot, which transiently accumulates large quantities of starch and proteins, is specifically dedicated to nutrient storage and remobilization, while the lateral roots are mainly dedicated to nutrient uptake. Proteomic data from the taproot and lateral roots highlighted the different senescence-related events that control nutrient remobilization and nutrient uptake capacities. Both the proteome and enzyme activities revealed senescence-induced proteases and nucleotide catabolic enzymes that deserve attention as they may play important roles in nutrient remobilization efficiency in rapeseed roots. Taking advantage of publicly available transcriptomic and proteomic data on senescent Arabidopsis leaves, we provide a novel lists of senescence-related proteins specific or common to root organs and/or leaves.

Keywords: Carbon, iron, lateral roots, nitrogen, proteases, rapeseed, root senescence, taproot.

Introduction

Senescence is the final stage in the development of plant organs. It has been mainly studied in leaves, where it is associated with the induction of numerous catabolic and proteolytic processes that participate in the degradation of macromolecules and ultimately in the dismantling of organelles. In leaves, catabolic events and chloroplast dismantling allow the release of numerous macro- and microelements that are essential for nutrient recycling and remobilization at the whole-plant level. Nutrient recycling and export from senescing organs is crucial for seed production and seed filling (Gregersen *et al.*, 2013; Avice and Etienne, 2014; Diaz-Mendoza *et al.*, 2016). This is why leaf senescence has been widely investigated in crops and model plants to identify the mechanisms and regulators involved in cell decay and chloroplast degradation. The

stay-green phenotype related to delayed senescence is one of the traits targeted by breeders to control carbon fixation and nutrient remobilization, and to improve seed yield and seed quality (Gregersen *et al.*, 2013; Lee and Masclaux-Daubresse, 2021). Transcriptomic studies of leaf senescence identified numerous transcription factors belonging to the WRKY, NAC, and ERF families (Guo *et al.*, 2004; Cao *et al.*, 2023), which control the switch from anabolic to catabolic metabolism. From these studies of gene expression patterns, senescence-associated genes (SAGs) and senescence-down-regulated genes (SDGs) were identified, which provided a comprehensive picture of the leaf senescence program. Among these SAGs, master actors in the degradation of cellular components were identified (Avice and Etienne, 2014; Havé *et al.*, 2017). The decrease of photosynthesis-associated genes, protease inhibitors, and transcription factors related to chloroplast maintenance was associated with leaf senescence (Breeze *et al.*, 2011).

Root senescence remains largely understudied compared with leaf senescence. The few reports on this topic describe root senescence as an age-dependent process leading to root browning, reduced nutrient uptake from the soil, and programmed cell death in the root cortical cell layer (Eissenstat, 2000; Bingham, 2007; Schneider and Lynch, 2018). Barley roots have been shown to undergo a genetically determined intrinsic senescence program that is mainly influenced by plant age and shares features with leaf senescence (Liu *et al.*, 2019). The similarities with leaf senescence reside in the involvement of the same transcription factor families, NAC, WRKY, and ERF, in the control of root and leaf senescence. The loss of physical integrity in roots is likely to be modulated by abscisic acid and cytokinin, as in leaves.

Roots can represent an important nutrient reservoir in many plant species such as perennials, meadow plants, and especially taproot plants. As an example, rapeseed is a nitrogen-demanding plant whose taproot stores proteins that represent a substantial nutrient reservoir and a nitrogen source to be remobilized during seed filling (Rossato *et al.*, 2002b; Gombert *et al.*, 2010; Girondé *et al.*, 2015). Indeed, while nitrate uptake decreases in rapeseed lateral roots after flowering, it was shown that the proteins accumulated in the taproot at the vegetative stage are hydrolyzed at the reproductive stage to support nitrogen export to the reproductive organs and especially to the seeds (Rossato *et al.*, 2002b).

Few studies have shown that root nitrogen remobilization was associated with protease induction (Kohli *et al.*, 2012) and root senescence, which involve the induction of amino acid transporters and glutamate catabolic enzymes (Wojciechowska *et al.*, 2018). Additionally, previous studies indicate that the senescence-associated gene 12 protease (SAG12), a cysteine protease previously identified in senescing leaves (Buchanan-Wollaston, 1997; Desclos *et al.*, 2009), is essential to promote root-to-seed protein remobilization in nitrogen-deprived Arabidopsis (James *et al.*, 2018, 2019). Consequently, it can be assumed that the remobilization of root nitrogen is associated with a senescence process that shares some molecular players with leaf senescence. However, it cannot be excluded that some processes may be specifically related to root senescence, particularly in the taproot, which plays a special role as a storage organ.

Therefore, the aim of this study was to monitor the onset and progression of root senescence associated with the remobilization of reserves during seed filling in rapeseed and to identify key players involved in it. The progression of root senescence was monitored using changes in anatomical and cellular structure already described as markers of root senescence in other plant species (Liu *et al.*, 2019). Reserve remobilization, proteolytic activities, and in-depth proteomic analysis of the taproot and lateral roots were performed to provide a comprehensive picture of the main events occurring in both root types during aging. Additionally, a comparison of the proteomic datasets with publicly available transcriptomic and proteomic data on leaf senescence in Arabidopsis was performed to identify leaf-common or root-specific senescence actors. Finally, the possibility to provide a set of molecular markers to better assess the course of root senescence is discussed.

Materials and methods

Plant material

Seeds of *Brassica napus* var. Aviso were germinated on perlite over demineralized water for 4 d in the dark, followed by 6 d under natural light. After the emergence of the first true leaf, seedlings were transferred to a 10 liter tank (10 seedlings per tank) containing the following nutrient solution: 3.75 mM NO_3^- nutrient solution [1.25 mM $Ca(NO_3)_2{\cdot}4H_2O$, 1.25 mM KNO_3, 0.5 mM $MgSO_4$, 0.25 mM KH_2PO_4, 0.2 mM EDTA·2NaFe·$3H_2O$, 14 µM H_3BO_3, 5 µM $MnSO_4$, 3 µM $ZnSO_4$, 0.7 µM $(NH_4)_6Mo_7O_{24}$, 0.7 µM $CuSO_4$, 0.1 µM $CoCl_2$] renewed every week for 22 d. At 32 days after sowing (DAS), plants were transferred to two contrasting nitrogen conditions: high nitrogen (HN; 3.75 mM N) and low nitrogen (LN; 4.2 µM N) conditions. The LN condition was chosen as it corresponds to a nitrogen-limiting condition known to reduce growth, exacerbate leaf senescence, and increase root expression of SAG12 and nitrogen remobilization from roots to pods (Desclos *et al.*, 2009; James *et al.*, 2018, 2019). After this, plants continued to grow in a greenhouse with a thermoperiod of 20/17 °C day/night and a photoperiod of 16 h with a mean photosynthetically active radiation of 350 µmol photons m^{-2} s^{-1} at canopy height (natural light supplemented with high-pressure sodium lamps Philips MASTER Green Power T400W Amsterdam, the Netherlands). At 47 DAS, plantlets were subjected to a 60 d period of vernalization in a climatic chamber maintained at 4 °C with artificial light (220 µmol photons m^{-2} s^{-1}) during the day (10 h day/14 h night). At 108 DAS, vernalization was stopped and plants were transferred to the same growth conditions as before the vernalization, but each plant was grown in an individual hydroponic pot of 4 liters for 57 d until the end of the flowering of the principal stem (at 164 DAS). At 108 DAS (vernalization output; C1, T0), 130 DAS (beginning of flowering; F1, T1), and 165 DAS (pod development; G4, T2), plants were harvested. A portion of root tissues was frozen in liquid nitrogen and stored at −80 °C for further biochemical analysis, and the remainder was stored in an oven (60 °C, 4 d) to obtain dry weight for biomass determination.

Microscopy observation

The lateral root tissues were included in low melting point agarose (5%; w/v) and cut with a vibratome (Microm 650v; Thermo Scientific; USA) before observation with a light microscope (AX70 Olympus and Olympus SC30 camera, Japan) with the help of CellSens software. The strong lignification of taproot tissues did not permit the use of a vibratome as for lateral roots. Consequently, sections of 2 mm of taproot were fixed with 2.5% glutaraldehyde in 0.1 M phosphate buffer pH 7 for 1 h to several days at 4 °C. The sections were rinsed in 0.1 M phosphate buffer pH 7 three times and post-fixed for 2 h with 1% osmium tetroxide in 0.1 M phosphate buffer pH 7. The sections were rinsed in phosphate buffer three times. The cells were then dehydrated in a progressive bath of ethanol (70–100%), embedded in resin EMbed 812, and polymerized for 48 h at 60 °C. For tissue observation, 1 µm semi-fine sections cut with a ultramicrotome and stained with 0.5% toluidine blue (1% sodium borate) were made and observed with a classical light microscope (Olympus AX70 and Olympus SC30 camera, Japan). For ultrastructure observation, ultrathin sections of 80 nm were made and contrasted with uranyl acetate and lead citrate. The sections were observed with a JEOL 1011 transmission electron microscope, and images were taken with a Gatan Orius 200 camera and a digital micrograph.

Elementary analysis

All dried samples of taproot and lateral roots were ground to a fine powder using stainless steel beads in an oscillating grinder (Mixer Mill MM400 Retsch, Haan, Germany). As detailed previously by Maillard *et al.* (2016), the iron (Fe) concentration was quantified after acid digestion of dry weight samples (~40 mg) with high-resolution inductively coupled plasma MS (HR-ICP-MS, Element 2TM, Thermo Scientific) using internal and external standards. The nitrogen concentration was quantified on 2 mg of dried powder with an elemental analyzer (EA3000, EuroVector, Milan, Italy).

Extraction and quantification of soluble and insoluble proteins

Soluble proteins in McIlvaine buffer (McIlvaine, 1921) were extracted from 200 mg of frozen fresh root tissue ground in a mortar with 300 µl of citrate phosphate buffer [20 mM citrate, 160 mM phosphate, pH 6.8 containing 50 mg of polyvinylpolypyrrolidone (PVPP)]. After centrifugation at 20 000 *g* at 4 °C for 20 min, the supernatant was collected and the proteins were assayed. The pellet was kept to extract the insoluble proteins in McIlvaine buffer. The pellet was resuspended in thiourea/urea buffer. After 1 h of incubation with shaking at room temperature, the extracts were centrifuged twice at 20 000 *g* at 4 °C for 10 min, and the supernatant with insoluble proteins was collected. The concentrations of the soluble and insoluble protein extracts were determined in the supernatants by protein staining (Bradford, 1976) using BSA as a standard.

Determination of proteolytic activities

Protease activities were determined on the soluble protein extracts and using the Abcam Assay Kit (ab111750), which incorporates fluorescein isothiocyanate (FITC)-labeled casein as a general protease substrate. Protease activities were determined at pH 5.5 and 7.5, the pH conditions at which cytotolic and vacuolar protease activities proceed, respectively (Poret *et al.*, 2016). For this, 15 µg of soluble proteins were incubated in a 200 µl reaction volume containing 2 mM DTT and sodium acetate buffer (50 mM, pH 5.5) for cysteine proteases and aspartate proteases, or Tris-base buffer (50 mM; pH 7.5) for serine proteases. Protease class activities were obtained by pre-incubating the sample with the addition of 50 µM of a protease class-specific inhibitor in DMSO: E-64 for cysteine proteases, aprotinin for serine proteases, and pepstatin A for aspartate proteases. After 30 min of incubation at 37 °C, the fluorescence of peptide fragments was measured at an excitation/emission (Ex/Em) wavelength of 485/530 nm.

Determination of amino acid content

Amino acids were extracted from 100 mg of dry matter to which 1 ml of 80% ethanol was added. Samples were incubated under agitation at 80 °C for 15 min, then centrifuged at 2300 *g* at room temperature for 10 min. The supernatant was reserved. The pellet was resuspended in 1 ml of deionized water and incubated under agitation at 60 °C for 15 min followed by centrifugation at 2300 *g* at room temperature for 10 min, and the supernatant was collected with the previous one. This last step with 1 ml of deionized water was repeated a second time. The collected supernatant was dried in a concentrator. The pellet was re-suspended in 100 µl of deionized water. To 100 µl of extract, 1 ml of ninhydrin (2,2-dihydroxyindane-1,3-dione) reagent [3.9 mM $SnCl_2{\cdot}H2O$, 2% ninhydrin (w/v), 100 mM citrate buffer, pH 5.5, and 50% DMSO (v/v)] was added and incubated at 100 °C for 20 min. After stopping the reaction with ice, the samples were diluted with 5 ml of 50% ethanol, and the absorbance at 570 nm was measured using glycine as a standard.

Quantification of starch

Starch content was extracted from 50 mg of dry matter and analyzed using the 'Total Starch' enzymatic kit (Megazyme International, County Wicklow, Ireland). Briefly, starch was digested first with thermal stable α-amylase and then with amyloglucosidase after gelatinization at 100 °C. Residual glucose was determined spectrophotometrically at 510 nm using glucose oxidase/peroxidase and 4-aminoantipyrine (GOPOD reagent) and glucose as a standard. The weight of free glucose was converted to anhydroglucose using a multiplication factor of 162/180.

Shotgun proteomic analyses

Protein extraction was performed using phenol extraction as described in Belouah *et al.* (2020). Protein pellets were then solubilized with 6 M urea, 2 M thiourea, 30 mM Tris–HCl, pH 8.5, 10 mM DTT, and 0.1% Rapigest (Waters). Protein content was estimated using a 2D QuantKit (GE Healthcare) and adjusted to 2 µg $µl^{-1}$. A 20 µg aliquot of protein was digested and desalted as described in Belouah *et al.* (2020). A total of 400 ng of desalted peptide digest were injected on Thermo Qexactive Plus (Thermo) coupled to an Eksigent nanoLC ultra 2D (see Supplementary Protocol S1 for detailed parameters). Peptide identification was performed using Xtandem (piledriver 2015.04.01.1) against the *B. napus* refseq genome (https://www.ncbi.nlm.nih.gov/protein/?term=txid3708[Organism:exp]) and an in-house protein contaminant database (55 entries) as described in Balliau *et al.* (2018). The detailed parameters are described in Supplementary Protocol S2.

Protein inference and quantification were performed using i2masschroq software (http://pappso.inrae.fr/bioinfo/i2masschroq/; Valot *et al.*, 2011; Langella *et al.*, 2017). The protein E-value was set to 0.00001 with two distinct peptides with an E-value of 0.01, resulting in a false discovery rate (FDR) of 0.1 at the peptide–spectrum match (PSM) level, 0.11 at the peptide level, and 0.015 at the protein level. Quantification was performed as described in Balliau *et al.* (2018). For extracted ion chromatogram (XIC) quantification, peptides were retained if they were present in at least 90% of the samples and if the correlation for all peptides dependent on a protein was higher than 0.5. When the peptides of a protein were not present or not reproducibly observed in one or more conditions, spectral counting (SC) was used in place of XIC analysis. For SC quantification, proteins were retained if they were observed by a minimum of five spectra in one sample. The mass spectrometry (MS) proteomics data were deposited at the ProteomeXchange Consortium via the

PRIDE (Perez-Riverol *et al.*, 2022) partner repository with the dataset identifier PXD050894.

Proteomic data: statistics and data mining

Statistical analyses were performed using Perseus software (https://maxquant.net/perseus/). Global proteomic data were analyzed using ANOVA with developmental stage as a variable factor. For quantification of proteins by the XIC and SC method, statistical analyses were carried out on log_2-transformed protein abundance. Proteins with a Student's test FDR ≤0.05 were considered to be significantly differentially accumulated. Missing data for the proteins analyzed by the SC method were replaced from the normal distribution. No fold change (FC) threshold was applied because a small change in protease abundance can have a large impact on the proteome due to post-translational regulation and the large spectrum of protease substrates. Proteases were identified using the MEROPS database (https://www.ebi.ac.uk/merops/) and Gene Ontology (GO). The GO and predicted subcellular localization were provided by the PANTHER database (pantherdb.org) and SUBA5 site (https://suba.live/), respectively. The heatmap representation was performed with proteases that are differentially abundant over time with a Pearson clustering method using the ComplexHeatmap R package (v2.13.3). GO enrichment analyses with the *B. napus* L. genome as a background were performed using Cytoscape (v3.9.1) plug-in ClueGO (v2.5.9; Fischer test with FDR correction) (Bindea *et al.*, 2009) or Pantherdb (https://www.pantherdb.org/; Fischer test with FDR correction) (Mi *et al.*, 2019). GO enrichment analyses with the Arabidopsis genome as a background were performed using VirtualPlant1.3 (Fischer test with FDR correction) (Katari *et al.*, 2010). Results focused on terms identified with a *P*-value <0.05. A meta-analysis of the proteomic data obtained in this study on the lateral roots and taproot of LN rapeseed plants was performed using the proteomic (Tamary *et al.*, 2019) and the transcriptomic (Breeze *et al.*, 2011) data obtained on Arabidopsis leaves with aging. The leaf senescent proteome from Tamary *et al.* (2019) was obtained from PRIDE with dataset identifier PXD010465; it provides data on protein accumulation in Arabidopsis leaves at four time points based on chlorophyll level. The transcriptome of leaf senescence published by Breeze *et al.* (2011) was obtained from NCBI's Gene Expression Omnibus (Edgar *et al.*, 2002) with GEO Series accession number GSE22982; it provides gene expression at 11 time points during the Arabidopsis leaf life span.

Statistical analysis

For all parameters, at least three biological replicates were measured ($n \geq 3$). All data are presented as the mean ±SE. To compare different data between different times or treatments, Tukey tests were performed after verifying compliance of normality with the Shapiro–Wilk test with R software. Data were log transformed if they did not follow a normal distribution. Statistical significance was postulated at $P \leq 0.05$.

Results

Phenotype of plants under high and low nitrate conditions

Regardless of the developmental stage (T0, T1, or T2), the LN plants developed fewer leaves with smaller size and a reddish phenotype compared with the HN plants (Fig. 1). At the flowering stage (T1), the number of flowers was lower in LN plants than in HN plants. However, all the HN and LN plants produced pods (Fig. 1). Both lateral roots and the taproot showed an increasing brownish color over time, which was particularly noticeable at pod filling stage T2 (Fig. 1). The smaller size of LN plants observed in Fig. 1 was in good agreement with the 5-fold lower biomass of LN plants compared with HN plants at T2 (17.58 g versus 95 g; Fig. 2A, B). In LN plants, limitation of biomass was observed on all the organs except lateral roots (Fig. 2A, B). Nevertheless, the partitioning of biomasses in the root was twice as high in LN plants than in HN plants (33.7% versus 18.6% at T0; 35% versus 16.8% at T1; and 26.7% versus 12.8% at T2, respectively; Fig. 2A, B). This shows that under nitrogen starvation, shoot growth has been neglected compared with root biomass.

Anatomical analysis of taproot and lateral roots

Lateral root tissues were examined by light microscopy after Evan blue staining to monitor cell viability (Fig. 3). At T0, which corresponds to the end of vernalization, the root cross-section was a regular circle and the LN and HN lateral roots differed mainly in root diameter, cell size, and number of cell layers in the cortex (4–5 for HN, 3 for LN). There was no evidence of cell death at T0 (Fig. 3A, D).

At flowering (T1) and pod filling (T2) stages, the shape of the cortical and epidermal cells was strongly affected, losing roundness especially in the outer layers and in the HN root. Their slight blue color at T1 intensified at T2, showing that cell death increased with age (Fig. 3B, C, E, F). In contrast, the integrity of the stele and vascular tissues was rather well preserved with aging in both HN and LN roots.

Observation of taproot tissue by light microscopy did not show any change in the cell shape with time but revealed a decrease in cell cohesion in both the HN and LN taproots (Fig. 4A–C, G–I). Both LN and HN taproot cells contain numerous organelles, identified as amyloplasts, whose number decreased between T0 (Fig. 4A, G) and T1 (Fig. 4B, H). These structures were completely absent at the T2 pod-filling stage (Fig. 4C, I). Ultrastructural imaging showed that amyloplasts were intact at T0 with a high stromal starch concentration (Fig. 4D, J), but decayed at T1 and T2. At T1, they had lost their structural integrity and starch, their size was greatly reduced, and they contained crystal structures that were not observed at T0. At T2, amyloplasts were dramatically shrunken and appeared as dislocated bodies that still contain numerous crystal structures but no more starch (Fig. 4E, F, K, L). The crystal structures in degenerating amyloplasts were identified as crystalloid ferritin structures by comparison with previous observations made on the chloroplasts of *Mesembryanthemum crystallinum* (Paramonova *et al.*, 2007). In taproot cells, crystalloid ferritin accumulated with aging under both LN and HN conditions (Fig. 4E, F, K, L). In good accordance we measured the increase in the taproot iron concentrations between T1 and T2 under both HN and LN conditions (Supplementary Fig. S1).

The decrease in starch observed with aging under microscopy paralleled amyloplast decay and was confirmed by starch

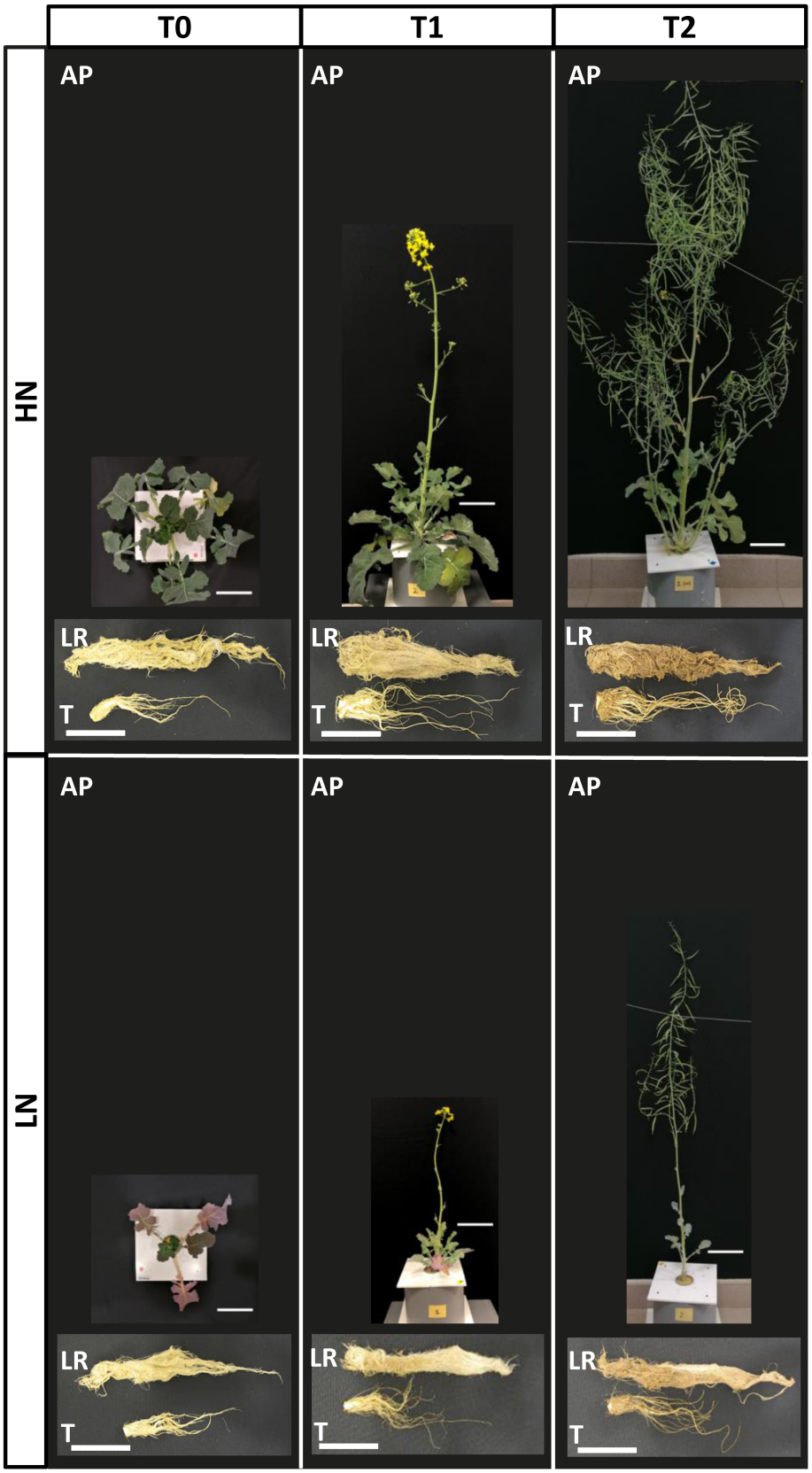

Fig. 1. Development of rapeseed cultivated under high (HN) and low nitrogen (LN) conditions. The different harvest times T0, T1, and T2 correspond to vernalization output (B9), beginning of flowering (F1), and pod development (G4) stages, respectively. AP, aerial parts; LR, lateral roots; T, taproot. The scale bars represent 10 cm.

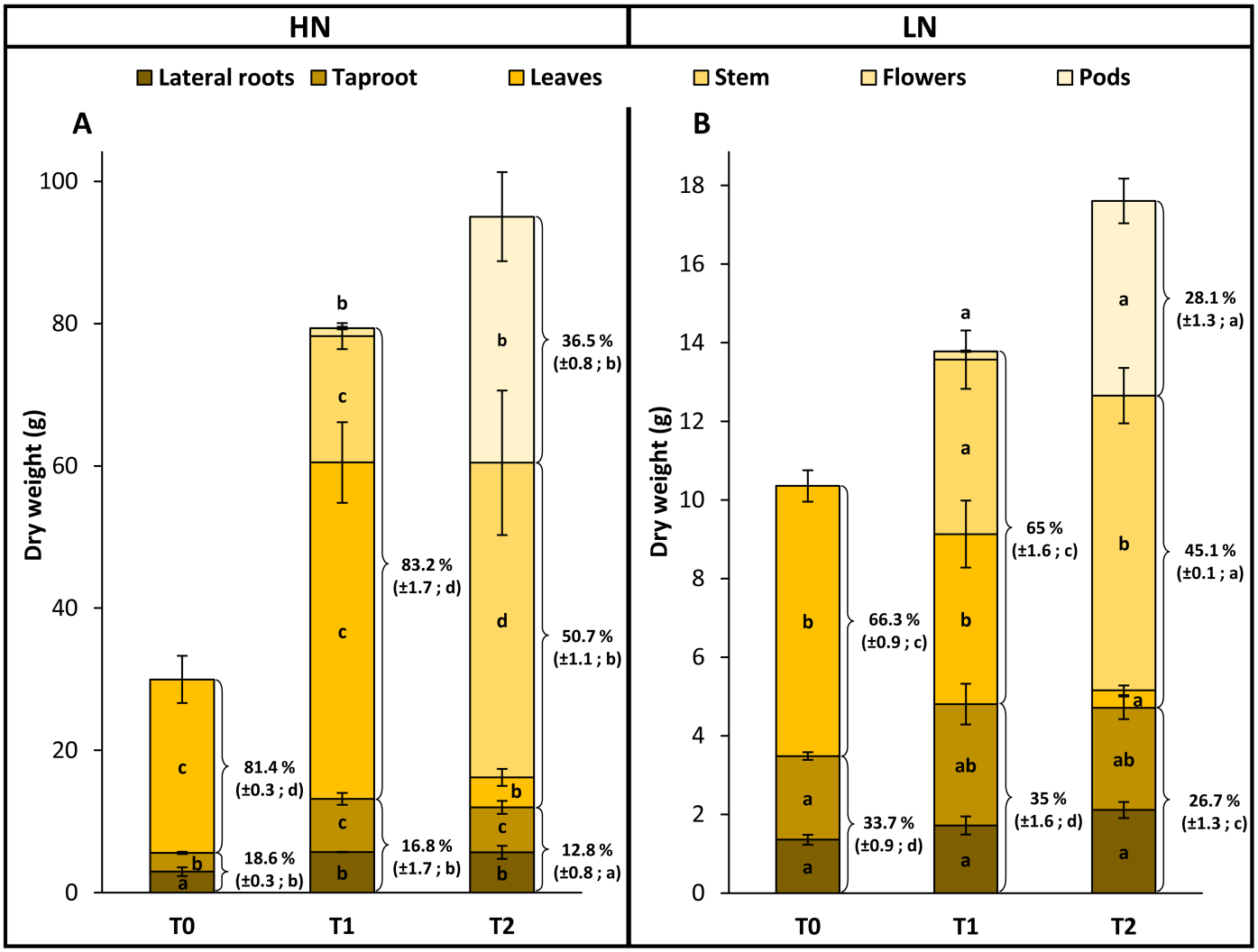

Fig. 2. Biomasses of whole plants and of the different compartments of rapeseeds. Plants were cultivated under high (HN; A) or low nitrogen (LN; B) conditions and harvested at T0, T1, and T2 corresponding to vernalization output (B9), beginning of flowering (F1), and pod development (G4) stages, respectively. Each color in a histogram bar correspond to the biomass of each plant compartment (means ±SE; *n*=3). The brackets to the right of the histogram bars correspond to the root (lateral roots and taproot), aerial (leaves, stems, flowers), and pod parts, and the associated values are the percentage (±SE; *n*=3) of each part relative to the total biomass. For a given compartment or a given part of the plant and regardless to the nitrogen condition, different letters indicate significant differences between developmental stages (*P*-value ≤0.05).

measurement assays (Fig. 4M, N). At the end of vernalization (T0), starch concentrations were similar in HN and LN taproots (21.3% and 22.3% of total taproot biomass, respectively). Starch concentrations decreased with aging in both LN and HN taproots, and to a greater extent in the HN tissues (Fig. 4M, N).

Aging effect on nitrogen, proteins, and amino acid contents in the taproot and lateral roots

The amounts of total nitrogen, proteins (soluble and insoluble), and free amino acids were higher in the lateral roots and taproots of HN plants than in LN plants (Fig. 5A–F). In lateral roots and taproots of HN plants, the amount of total nitrogen increased 2-fold between T0 and T1 (Fig. 5A, B), and was reduced by one-third for the taproot and one-quarter for the lateral roots between T1 and T2. In LN plants, the amount of nitrogen was globally kept constant (~25 mg per organ) throughout the entire aging process in both taproot and lateral roots (Fig. 5A, B).

At T0, the amounts of soluble and insoluble proteins were approximately the same in the taproot and lateral roots of HN plants (~150, 95, and 55 mg, respectively; Fig. 5C, D). In the taproot of HN plants, the amount of soluble proteins increased 2-fold and insoluble proteins increased 3-fold between T0 and T1. Subsequently, soluble and insoluble proteins decreased by 70–75% between T1 and T2 (Fig. 5C). In the lateral roots of HN plants, only insoluble proteins increased significantly

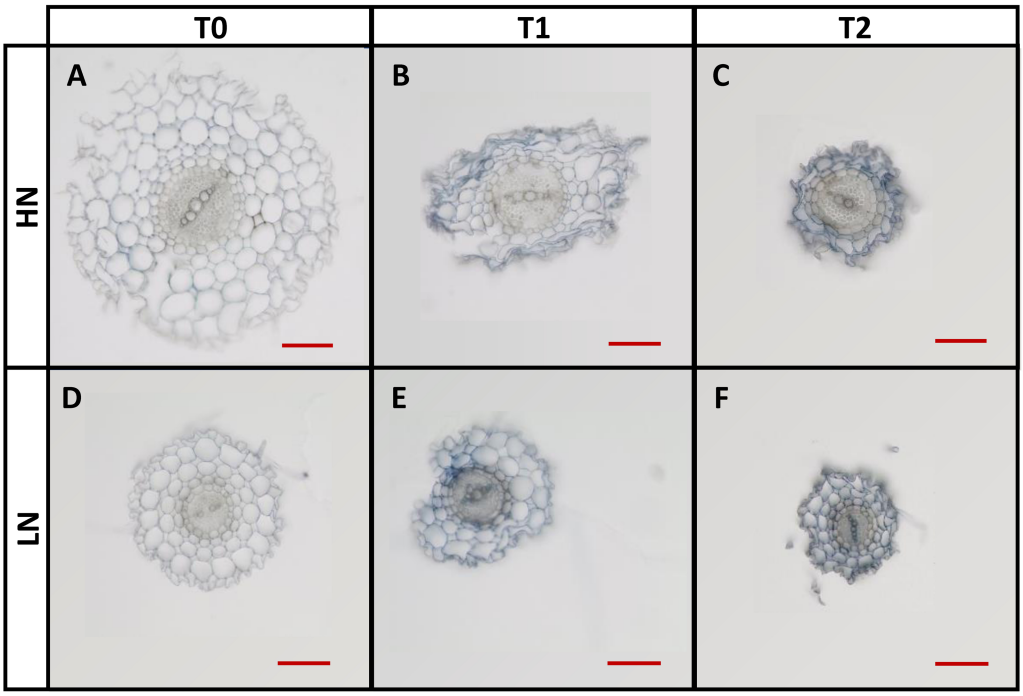

Fig. 3. Structural changes in the cortex of rapeseed lateral roots over time under high (HN) or low nitrogen (LN) conditions. Pictures of root tissue sections, observed after staining with Evans blue using a light microscope, were obtained at vernalization output (T0; A, D), beginning of flowering (T1; B, E), and pod development (T2; C, F) under HN (A, B, C) or LN (D, E, F) conditions. The red scale bars represent 100 µm. Representative pictures are shown, *n*=3.

between T0 and T1 (Fig. 5C). Under HN, total proteins decreased by 48% in lateral roots (Fig. 5D) between T1 and T2 and by 74% in taproot (Fig. 5C). Under LN, total protein level was maintained in lateral roots; it significantly decreased in taproot between T1 and T2 (Fig. 5C, D). Regardless of the nitrogen treatment, the decrease in total protein content in lateral roots is related to the decrease in soluble protein, while in the taproot both insoluble and soluble protein equally decrease with aging (Fig. 5C, D).

Changes in free amino acid content in the taproot (Fig. 5E) are quite similar to those of proteins (Fig. 5C). In the taproot of HN plants, amino acids increased by 1.8-fold between T0 and T1 and then decreased by 2.2-fold between T1 and T2. In the LN taproots, amino acid content steadily decreased by 2-fold from T0 to T2, while it was maintained at the same level in the LN lateral roots (Fig. 5F). There was no significant change in amino acid content in HN lateral roots with aging (Fig. 5F).

Protease activities in taproot and lateral roots

Total protease and specific protease activities (cysteine, aspartic, and serine proteases) measured at pH 5.5 or 7.5 were lower in taproot than in lateral roots (Fig. 6A, F). In taproot, protease activities were not different between HN and LN; they were very low at T0 and T1 and sharply higher at T2 (Fig. 6A–E). In lateral roots, total and specific protease activities increased gradually with aging (Fig. 6F–J). This increase was higher under LN compared with HN, showing that nitrate limitation stimulated an increase in protease activities. In both taproot and lateral roots, protease activities were mainly represented by the cysteine and aspartic proteases (Fig. 6).

Proteomic analysis on taproot and lateral roots of plants grown under LN conditions

To identify root senescence markers and provide a comprehensive picture of root aging, shotgun proteomic analyses were performed on the taproot and lateral roots of plants grown under LN at T0, T1, and T3 (Supplementary Tables S1–S4). Analyses were performed on LN roots as they exhibited higher changes in protease activities than HN roots and should provide a good picture of senescence and nutrient remobilization processes (Fig. 6).

The shotgun proteomics identified a total of 3028 and 2523 (Supplementary Tables S5, S6) significantly differentially accumulated proteins (DAPs) depending on the developmental stage in the taproot and lateral roots, respectively (ANOVA; FDR ≤0.05). GO exploration using Cytoscape (v3.9.1) and the plug-in ClueGO (v2.5.9) (Bindea *et al.*, 2009) identified 29 significant biological processes for the taproot and lateral root DAPs. Amongst the most significant that are shown in Fig. 7A and B, several (12 and 13 for taproot and lateral root, respectively) are closely related to nitrogen metabolism and common to both root organs. Interestingly, four enriched biological

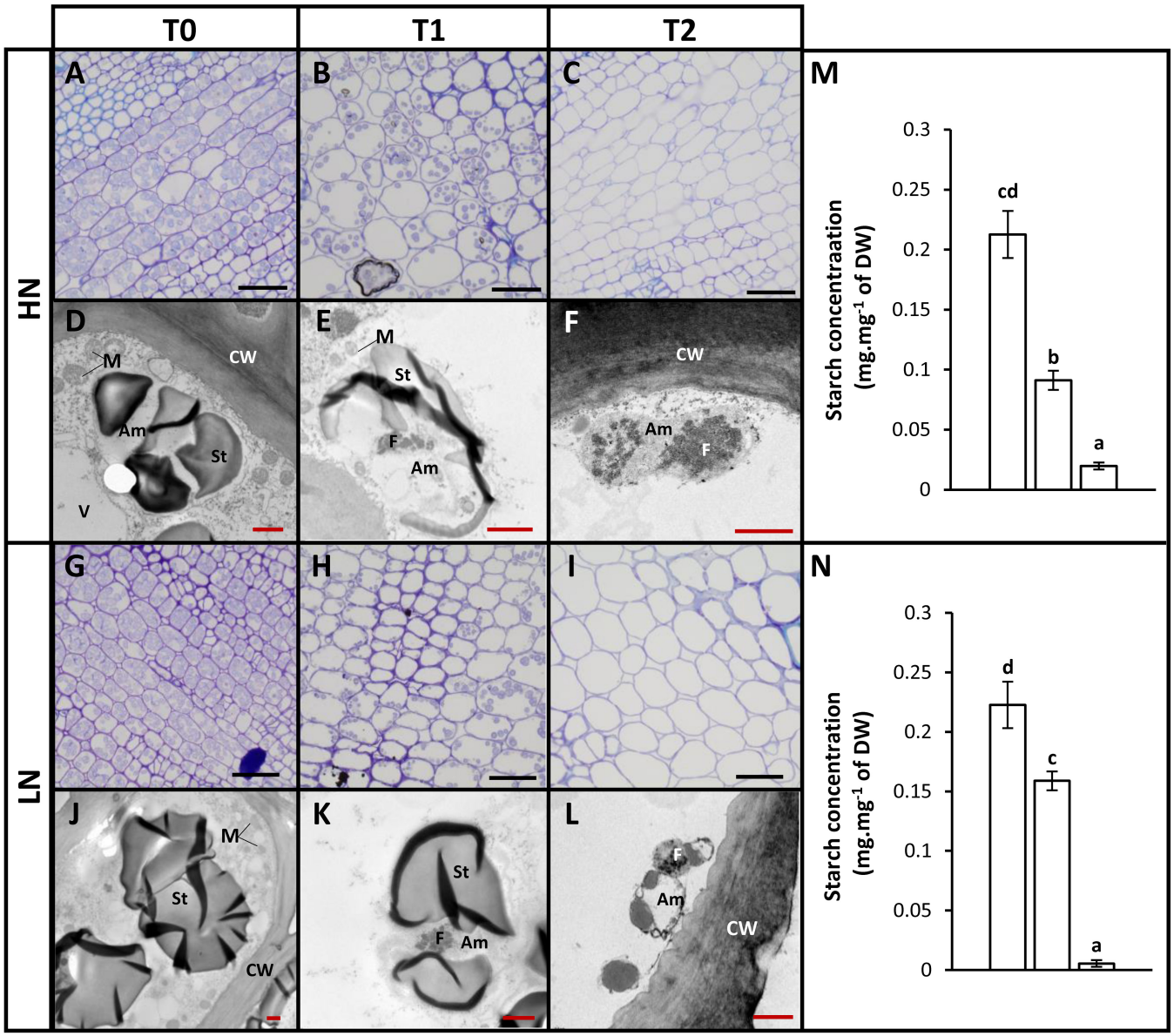

Fig. 4. Structure, ultrastructure, and starch concentration changes in the taproot tissues during the development of rapeseed cultivated under high (HN) or low nitrogen (LN) conditions. Taproot structure was obtained after staining with 0.5% toluidine blue (1% sodium borate) using a light microscope at vernalization output (T0; A, G), beginning of flowering (T1; B, H), and pod development (T2; C, I) under HN (A–C) or LN (G– I) conditions. Cellular ultrastructure was obtained after staining with 1% osmium tetroxide by using a transmission electron microscope at vernalization output (T0; D, J), beginning of flowering (T1; E, K), and pod development (T2; F, L) under HN (D– F) or LN (J– L) conditions. Black and red scale bars correspond to 50 µm and 1 µm, respectively. Am, amyloplast; CW, cell wall; F, ferritin deposits; M, mitochondria; St, starch grain; V, vacuole. Starch concentrations in taproots were measured over time under HN (M) or LN (N) conditions. Values are means ±SE (n=3). Significant differences between development stages regardless of the nitrogen condition are indicated by different letters (P-value ≤0.05).

processes related to catabolism and metabolism of organonitrogen compounds include many proteases, some of which have been identified in *B. napus* leaf senescence by Poret *et al.* (2019) (Supplementary Tables S8, S9).

Detoxification processes, which are consistent with senescence and catabolism, are specifically enriched in the taproot and in lateral roots, but with lower significance (Fig. 7; Supplementary Tables S8, S9). Thus, taproot and lateral roots share several biological processes related to organic acid metabolism (oxoacid and carboxylic acid metabolism), amino acid biosynthesis, nucleobase biosynthesis, proteolysis, and catabolism.

Clustering was performed to get a better insight into proteomic changes in taproot and lateral root. Heatmaps identified four main clusters for both taproot and lateral roots which had similar patterns (Fig. 8A–C; Supplementary Tables S5, S6). Cluster 1 corresponds to proteins whose

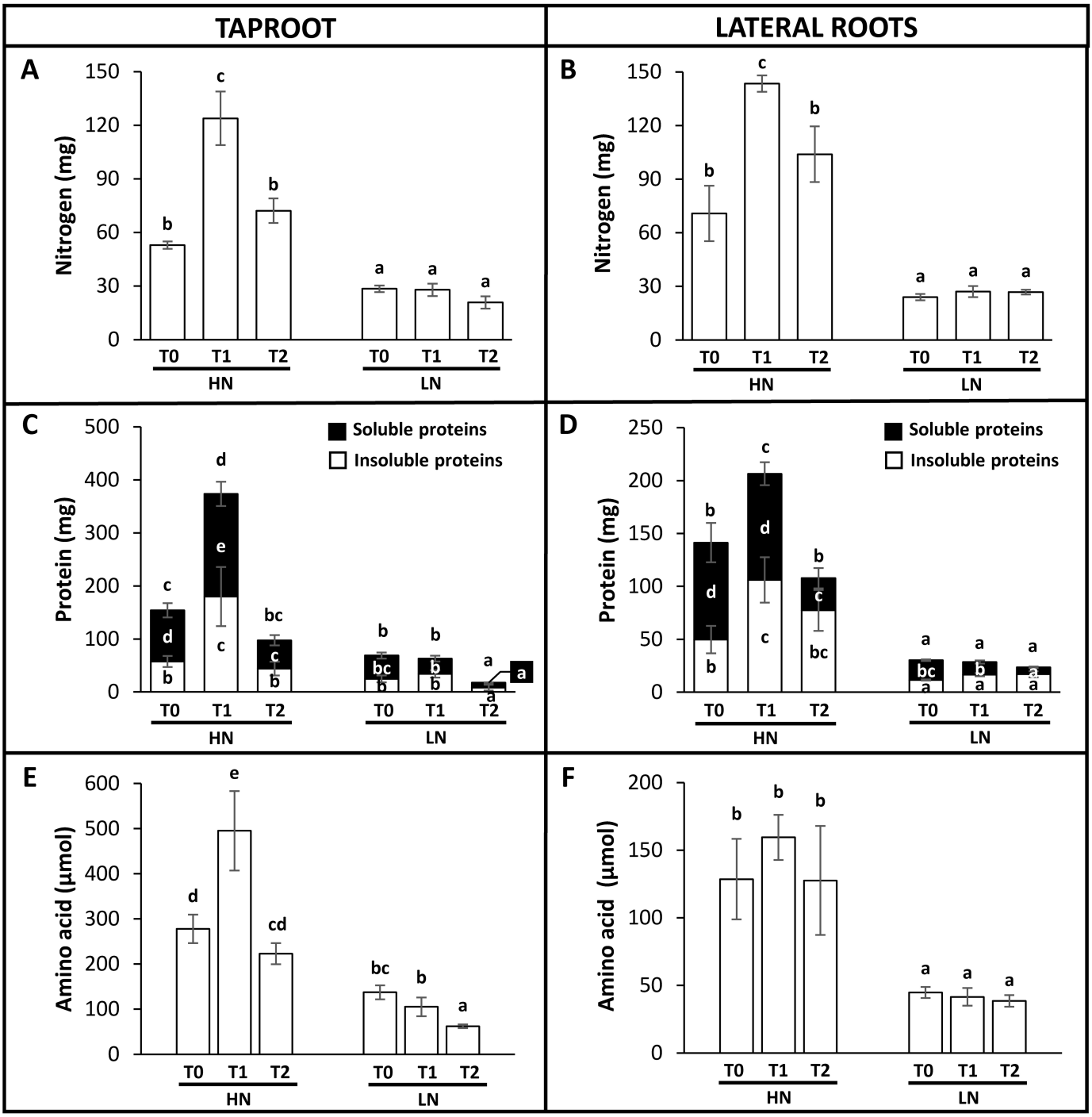

Fig. 5. Total nitrogen, protein, and amino acid amounts in the taproot and lateral root tissues during the development of rapeseed cultivated under high (HN) or low nitrogen (LN) conditions. The different harvest times T0, T1, and T2 correspond to vernalization output (B9), beginning of flowering (F1), and pod development (G4) stages, respectively. Total nitrogen (A, B), soluble and insoluble proteins (C, D), and amino acid (E, F) amounts were measured in taproot (A, C, E) and lateral roots (B, D, F) over time under HN or LN conditions. Values are means ±SE (n=3). For a given root tissue, different letters indicate significant differences (P-value ≤0.05) regardless of the nitrogen condition and developmental stages.

abundance decreases late at T2 (T1≥T0>T2). Cluster 2 corresponds to proteins whose abundance decreases early from T1 (T0>T1>T2). Cluster 3 includes proteins with similar abundance at T0 and T1 and a significant increase in abundance at T2 (T0–T1<T2). Cluster 4 corresponds to proteins whose abundance increases early at T1 and continues to increase at T2 (T0<T1<T2). Thus, clusters 1 and 2 correspond to proteins significantly depleted with senescence

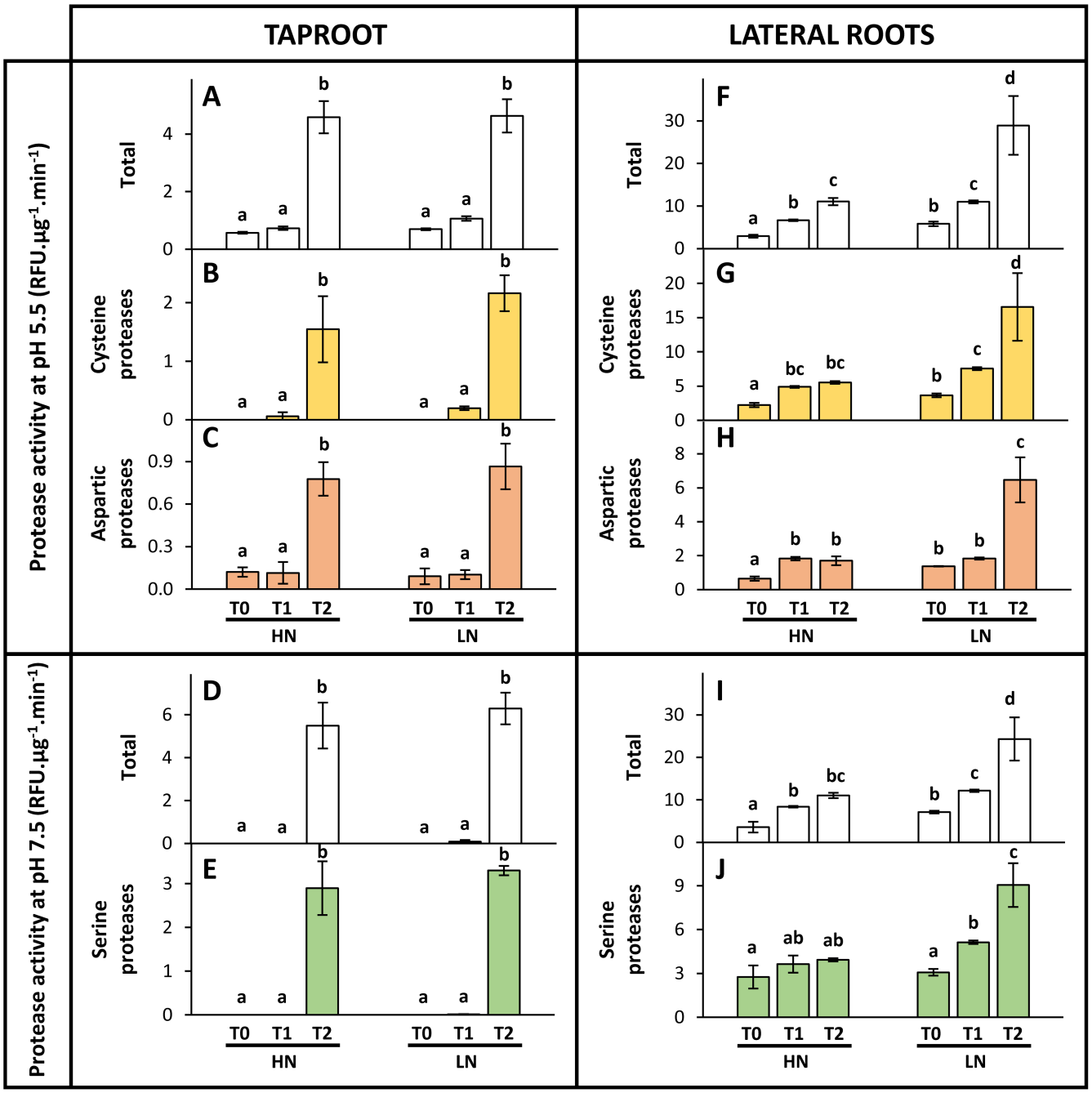

Fig. 6. Activities of total and specific proteases in the taproot and lateral root tissues during the development of rapeseed cultivated under high (HN) or low nitrogen (LN) conditions. The different harvest times T0, T1, and T2 correspond to vernalization output (B9), beginning of flowering (F1), and pod development (G4) stages, respectively. The total protease activities at pH 5.5 (A, F) and pH 7.5 (D, I), the cysteine (B, G) and the aspartic (C, H) protease activities at pH 5.5, and the serine protease activities at pH 7.5 (E, J), were measured in taproot (A–E) and lateral roots (F–J) over time under HN and LN conditions. Protease activities are expressed in relative fluorescence units (RFU) per µg of protein per minute. Values are means ±SE (n=3). For a given root tissue, different letters indicate significant differences (P-value ≤0.05) regardless of the nitrogen condition and developmental stages.

(SDP; senescence-depleted protein) and clusters 4 and 5 to proteins significantly accumulated with senescence (SAP; senescence-associated protein). The proportions of SDP and SAP are almost the same regardless of the root organ (Fig. 8A, B).

UpSet plots of root and lateral root clusters differentiate proteins present in only one cluster (i.e. organ-specific) from proteins present in two different clusters (i.e. in both taproot and lateral roots) (Fig. 8C). The majority of the proteins present in two different clusters are either SDPs or SAPs in the two root

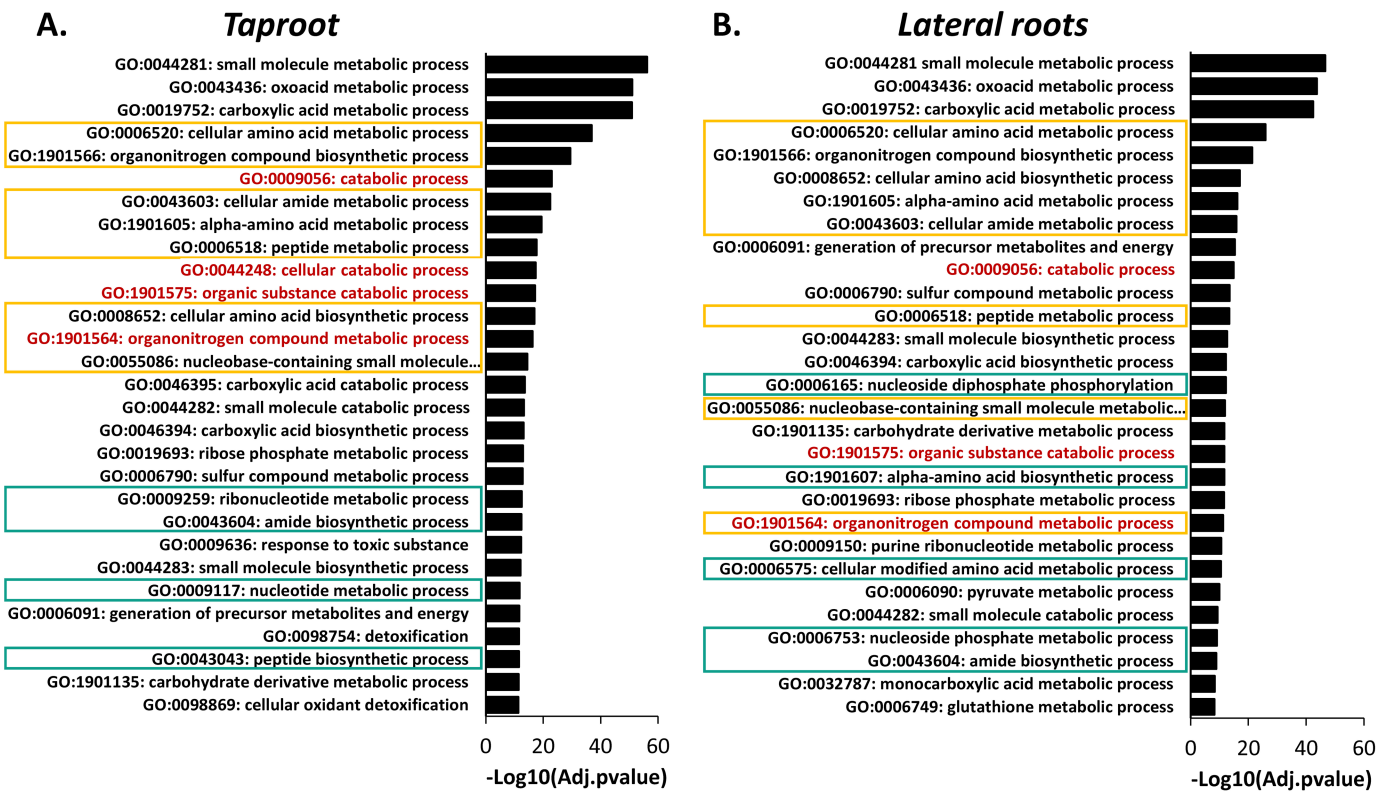

Fig. 7. Biological processes in the taproot and lateral root tissues during the development of rapeseed cultivated under low nitrogen (LN) conditions. Analysis of biological process categories significantly enriched using Cytoscape (v3.9.1) and the plug-in ClueGO (v2.5.9) (Bindea *et al.*, 2009) for the taproot (A) and lateral root (B) DAPs was performed and the 29 most significant GO terms are presented. Categories related to nitrogen metabolism common or specific to root organs are framed in yellow and green, respectively. Enriched biological processes written in red include many proteases known to be involved in leaf senescence.

types. Only a few are SDPs in the taproot and SAPs in the lateral root, or vice versa.

Biological processes enriched in the different situations presented in Fig. 8C and listed in Supplementary Table S10 reflect that the catabolism of amino acids, of cell wall, and of peroxide as well as detoxification processes were increased with aging in both taproot and lateral roots, while anabolic processes, translation, and DNA replication were more active in young roots. It can be noted that terms related to inorganic nitrate and sulfate assimilation were over-represented in the lateral roots, which are the site of mineral uptake.

Comparison of our *B. napus* root senescence proteome with transcriptomic and proteomic markers of senescing Arabidopsis leaves

To our knowledge, the proteomic and transcriptomic data obtained and published for leaf senescence in *B. napus* are limited or absent. Therefore, we decided to perform a meta-analysis combining the root proteomic data obtained in this study on *B. napus* with proteomic and transcriptomic data from *Arabidopsis thaliana*. Because it provides a rigorous classification and clustering of both leaf SAGs (leaf_SAG) and leaf senescence-repressed genes (SRGs; leaf_SRG), we chose to use the transcriptomic data of Breeze *et al.* (2011) for comparison. In the same spirit, we used the leaf proteome analysis of Tamary *et al.* (2019) to extract the Arabidopsis leaf senescence-overaccumulated proteins (leaf_SAP) and the leaf SDPs (leaf_SDP).

We could identify 157 orthologous Arabidopsis leaf SAGs/SAPs (leaf_SAPs and leaf_SAGs) for the taproot SAPs (taproot_SAPs) (Fig. 9A; Supplementary Table S5) and 117 for the lateral roots SAPs (LR_SAPs) (Fig. 9B; Supplementary Table S6). Amongst them, 88 are common to taproot, lateral roots, and leaf, 29 are common to lateral roots and leaf but not taproot, and 69 are common to taproot and leaf but not to lateral root (Fig. 9C; Supplementary Table S7). These proteins are the common leaf and root senescence markers.

We also identified 60 orthologous Arabidopsis leaf SRGs/SDPs (leaf_SRGs and leaf_SDPs) for the taproot SDPs (taproot_SDPs) (Fig. 9A; Supplementary Table S5) and 47 for the lateral root SDPs (LR_SDPs) (Fig. 9B; Supplementary Table S6). Amongst them, 29 are common to taproot, lateral roots, and leaf, 18 are common to lateral roots and leaf but not to taproot, and 31 are common to taproot and leaf but not to lateral roots (Fig. 9C; Supplementary Table S7). These proteins are the common leaf and root longevity markers.

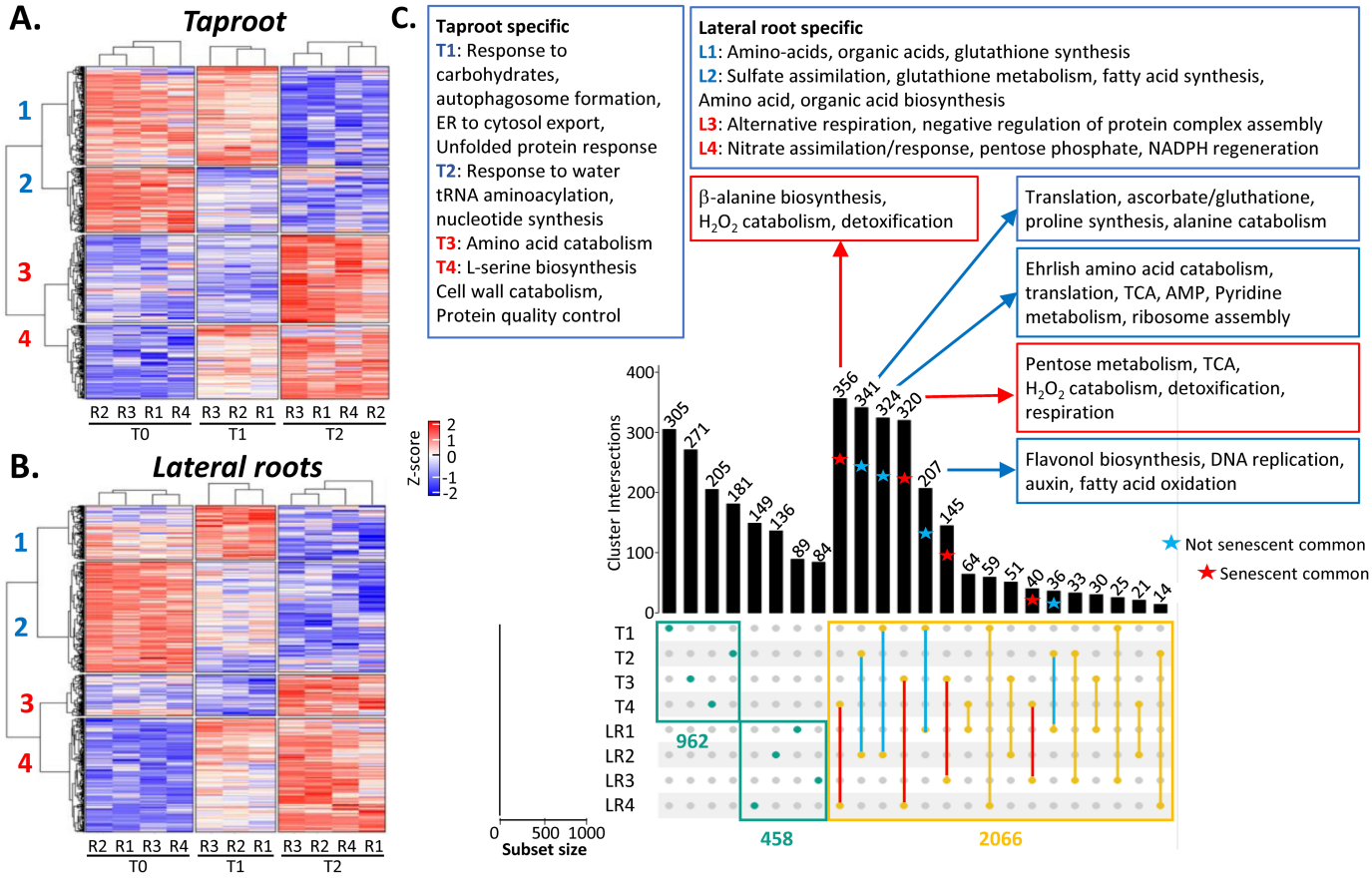

Fig. 8. Changes in biological processes with taproot and lateral root aging. The different harvest times T0, T1, and T2 correspond to vernalization output (C1), beginning of flowering (F1), and pod development (G4) stages, respectively. Heatmaps (A, B) represent the abundance of proteins (transformed in *Z*-score; red and blue for high and low accumulation, respectively) whose variability over time was confirmed by ANOVA in taproot (A) and in lateral roots (B). Each column corresponds to a biological replicate and the numbers at the left of the heatmap correspond to a cluster number. (C) UpSet plot identifies the time- and organ-specific DAPs (green spots) and those shared by taproot and lateral root (yellow spots). Senescence-related and early development (not senescent) common DAPs are identified by red and blue colors, respectively. Biological process enrichment was performed with all proteins presented in each UpSet plot group using Panther (https://www.pantherdb.org/). Significant enrichment (Fischer test with FDR correction) is presented. According to (A) and (B), subsets used for Upset plots in (C) are: T1, taproot cluster 1; T2, taproot cluster 2; T3, taproot cluster 3; T4, taproot cluster 4; L1, lateral roots cluster 1; L2, lateral roots cluster 2; L3, lateral roots cluster 3; L4, lateral roots cluster 4.

In addition, we identified (i) 36 and 21 senescence markers specific to the taproot and/or the lateral roots, respectively, that belong to the leaf_SDPs and leaf_SRGs of Arabidopsis, and (ii) 70 and 90 longevity markers specific to the taproot and/or the lateral roots, respectively, that belong to the leaf_SAPs and leaf_SAGs of Arabidopsis (Fig. 9A, B; Supplementary Table S7).

GO terms associated with the common leaf and root senescence markers were related to 'nucleobase catabolism' and 'response to oxidative stress' in both taproot and lateral roots, and to 'cysteine type endopeptidases' in taproot. GO of the common root and leaf longevity markers are related to 'C metabolism'. Root-specific senescence markers are associated with 'amino acid metabolism' and 'carbon metabolism', while the root-specific longevity markers are related to 'fatty acid degradation', 'oxidoreductase activities', and 'carboxylic acid catabolism'. It is interesting to note that GO terms are almost similar for taproot and lateral roots.

Identification of proteases in the proteome of taproot and lateral roots

Both the decrease in protein content (Fig. 5) and the increase in protease activities (Fig. 6) prompted us to analyze in more detail the SAPs and SDPs related to the proteolytic activities (proteases and proteasome-related proteins). A total of 165 and 112 proteases were identified in taproot and lateral roots, respectively, using the MEROPS database (https://www.ebi.ac.uk/merops/), and the protease list was manually curated using GO (Supplementary Tables S11, S12). According to the heat maps of the taproot and lateral root proteases (Supplementary Fig. S2), we can globally define two senescence-accumulated (95 for taproot and 46 for lateral roots) and senescence-depleted (70 for taproot and 66 for lateral roots) protease groups (Supplementary Fig. S2; Supplementary Tables S11, S12). The UpSet plot shown in

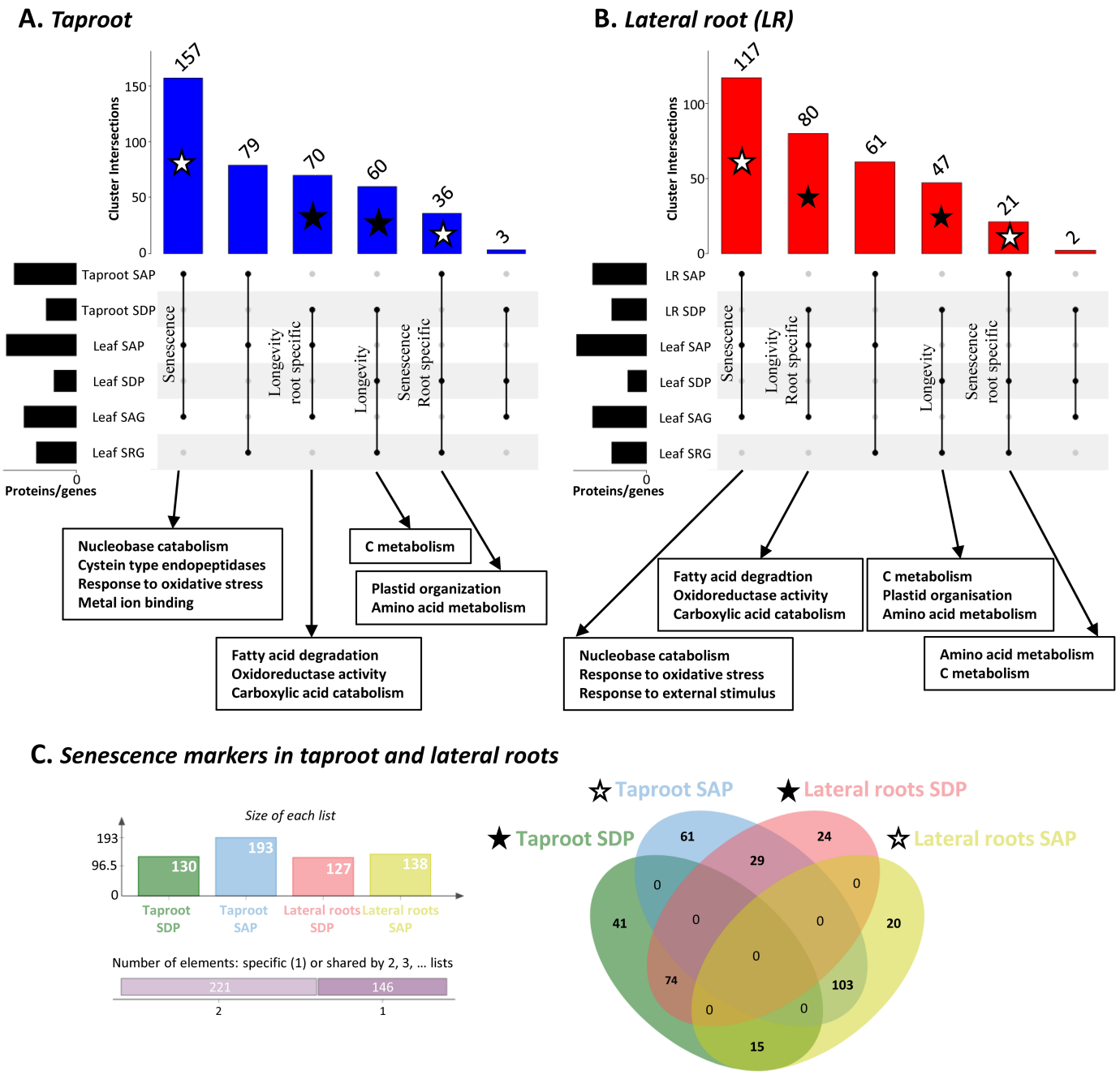

Fig. 9. Longevity and senescence markers in taproot and lateral roots. Arabidopsis orthologous genes of the *B. napus* taproot (A) and lateral root (B) senescence-associated (SAP) and senescence-depleted (SDP) proteins were identified amongst (i) the Arabidopsis senescence-associated (SAG) and senescence repressed (SRG) genes from Breeze *et al.* (2011) and (ii) the Arabidopsis SAPs and SDPs from Tamary *et al.* (2019). The number of orthologous genes corresponding to each category is indicated on the top of each bar. The stars represent the senescence markers (white stars) and longevity markers (black stars) in *B. napus* roots and/or Arabidopsis leaves. Functional categories over-represented in the set accessions are indicated next to the arrows (VirtualPlant1.3; FDR correction). (C) Venn diagram of the senescence protein markers (SDP and SAP) in taproot and lateral roots. LR, lateral roots; Tp, taproot.

Fig. 10 distinguishes between taproot-specific proteases, lateral root-specific proteases, and proteases common to both lateral roots and taproot. Very few common proteases were differentially affected by aging in taproot and lateral roots, and we will not comment on them. Most of the common proteases were either overaccumulated or depleted with senescence in both taproot and lateral roots. The 40 common senescence overaccumulated proteases were mainly represented by cysteine proteases (13) and equal numbers of aspartate, serine, and metallo-proteases. The 40 common

senescence-depleted proteases were mainly represented by the proteasome subunits (16), metallo-proteases (12), and serine proteases. These patterns were in good agreement with the senescence picture described for leaf senescence (Roberts *et al.*, 2012).

A total of 69 taproot-specific proteases (41 overaccumulated and 28 depleted with senescence) were identified, while the lateral root contained only 16 (Fig. 10). Among the 41 taproot senescence-related proteases, half are serine proteases and we can note the presence of well-known senescence-related cysteine proteases such as SAG12, RD21A, and RD21B (Roberts *et al.*, 2012). The taproot-depleted proteases are mainly represented by proteasome subunits and serine proteases.

Five of the six cysteine protease inhibitors identified in the taproot and lateral root DAPs were more abundant in young root tissues (Fig. 11). In contrast, Kunitz trypsin inhibitors, which normally regulate serine protease activities, were more abundant in the old root tissues. The opposite effect of senescence on the relative abundances of the different cysteine proteases and of their cognate inhibitors is consistent with a fine-tuned control of proteolytic activities during root development.

Discussion

Anatomical and physiological markers for root senescence

Determination of the onset of senescence is a difficult problem that has been addressed regarding leaf senescence in numerous studies that aimed to identify the best markers of the transition between mature and senescent leaves (Buchanan-Wollaston, 1997; Masclaux *et al.*, 2000). The stage at which the leaf reaches its optimal size was considered as the time of transition from the mature stage to the senescent stage. The decreases in chlorophyll and Rubisco contents and the increase

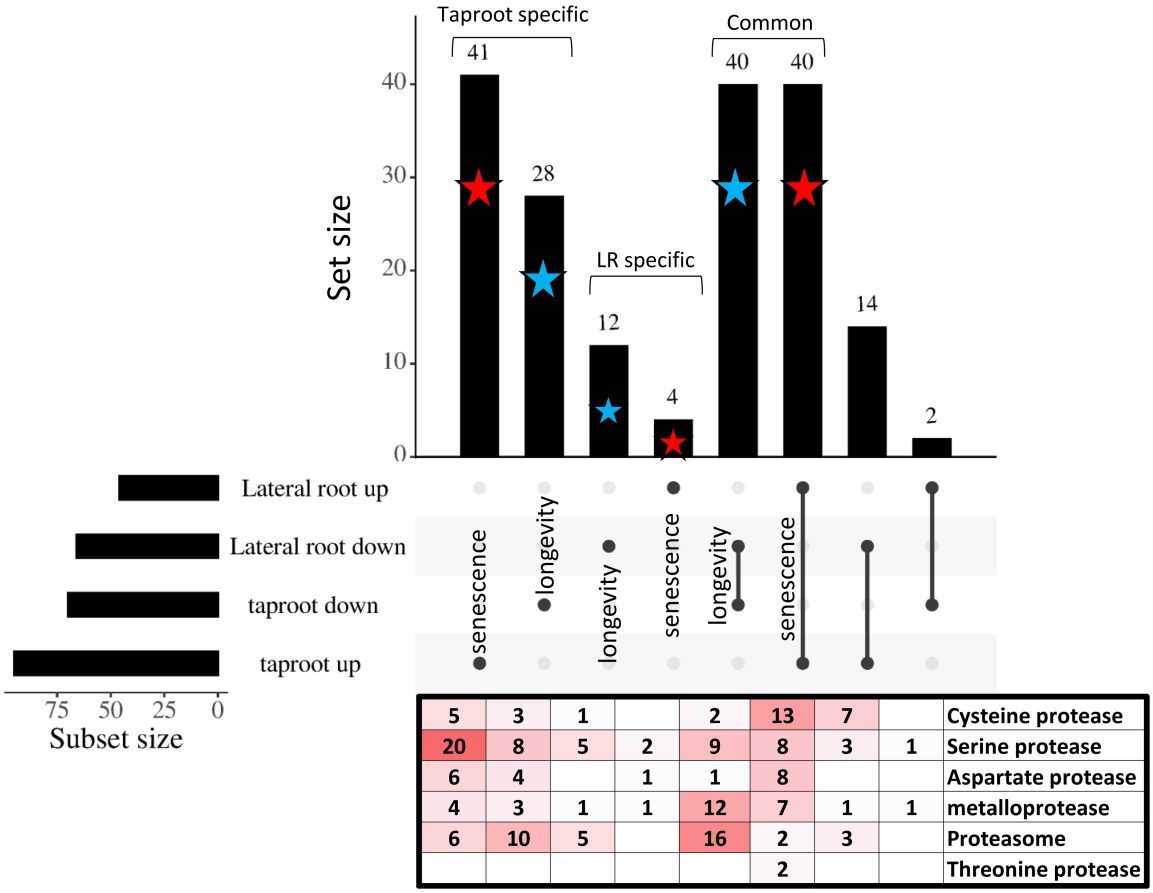

Fig. 10. Senescence- and longevity-associated proteases in taproot and lateral roots. Proteases of taproot and lateral roots were qualified as senescence associated (up) or longevity associated (down) depending on if they were up-accumulated or depleted with aging. Proteases specific for or common to taproot and lateral roots were identified, and the number of proteases corresponding to each category is indicated on top of each bar. The stars represent the senescence-associated proteases (red stars) and the longevity-associated proteases (blue stars). The number of cysteine, serine, aspartate, metallo-, and threonine proteases and of proteasome subunits associated with each category is indicated in the table. Red color intensifies with increasing numbers.

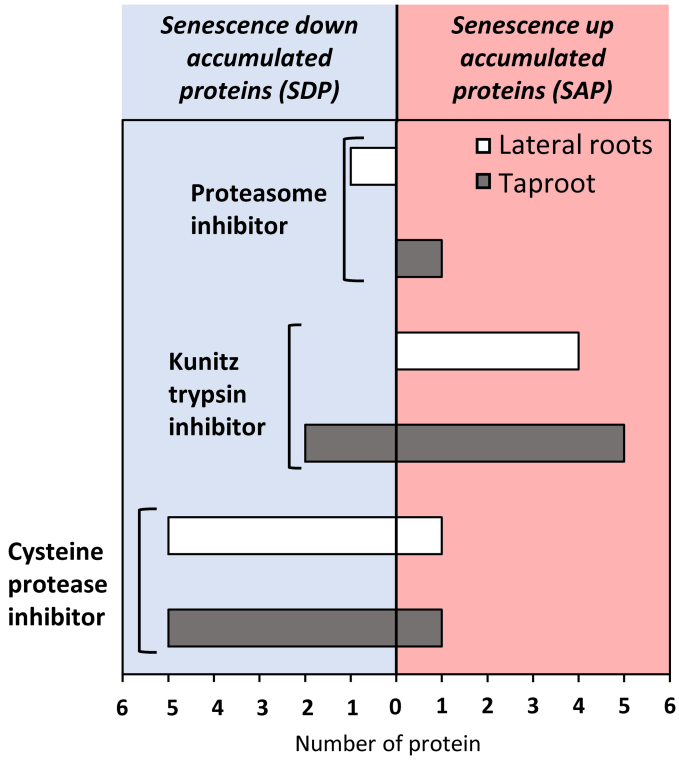

Fig. 11. Evolution of protease inhibitors in taproot and lateral roots. Protease inhibitors of taproot (gray bars) and lateral roots (white bars) up- or down-accumulated during taproot senescence. The size of each bar in the histogram is associated with the number of protease inhibitors identified. Three main groups of proteases inhibitors were found, proteasome inhibitor, Kunitz trypsin inhibitor, and cysteine protease inhibitor.

in protease activities were used as other measurable physiological markers of the leaf senescence stage. As all these indicators do not evolve in parallel; leaf senescence has been split into three stages: early, intermediate, or late senescence. Our results suggest that similar to leaves, there is not a unique senescence marker, rather a combination of markers that can define early and late senescence status.

The three stages chosen for this study cover the whole developmental cycle of *B. napus*. Between T1 and T2, a classical decrease in the biomass of vegetative organs was observed (Fig. 2), as previously described (Malagoli *et al.*, 2005; Girondé *et al.*, 2015). This decrease coincides with the formation of pods and the transfer of nutrients from the remobilization of plant resources to seed development. As such, decreased root biomass can be considered as senescence onset in the same way that a decrease in leaf area was considered as the onset of leaf senescence.

Browning of lateral roots and taproot that was appearing at T1 is another phenotype of root senescence that is related to changes in secondary metabolites and certainly to oxidation, and which has already been described in the literature (Liu *et al.*, 2019). Although browning started at T1, it became particularly pronounced at T2, and was thus more likely to be a late senescence marker (Fig. 1). Root browning has been reported in several studies on grape, peach tree, poplar, and cotton as a trait feature of the transition from an active to a senescent root (Comas *et al.*, 2000; Baldi *et al.*, 2010; Wojciechowska *et al.*, 2020; Zhu *et al.*, 2021). Our light microscopy observations showed that browning of the root structure (Fig. 3) was accompanied by cell deformation and loss of cortical cell viability in both LN and HN plants. The loss of cortical cell integrity has been described in several studies on *Poaceae* as a type of programmed cell death called root cortical senescence (RCS) (Schneider *et al.*, 2017; Schneider and Lynch, 2018; Liu *et al.*, 2019; Lynch, 2019). RCS has been known for a long time, and several authors (Henry and Deacon, 1981; MacLeod *et al.*, 1986; Schneider *et al.*, 2017) proposed that RCS may be analogous to the senescence of leaves and shoots as they share many similarities such as induction upon nutrient deficiencies, induction by ethylene, and the fact that RCS induces the accumulation of pathogenesis-related proteins as in early stages of leaf senescence. RCS described in *Poaceae* was shown to decrease root respiration and nutrient transport, and to affect water use efficiency. In contrast to lateral roots, no visual change in cell shape was observed over time in the taproot, regardless of nitrogen treatment (Figs 3, 4). However, changes in intracellular organization were observed for taproot cells. Indeed, at the end of the vernalization period, taproot cells accumulated a large amount of starch granules and amyloplasts (Fig. 4). Starch accumulation was independent of nitrate status, in good agreement with Rossato *et al.* (2002a). Starch concentration in the vernalized taproot was 21.3% and 22.3% of the dry biomass in the HN and LN conditions, respectively. The starch concentration was 14 times higher than that measured in the lateral roots (Supplementary Fig. S3), confirming the importance of the taproot as a carbon storage compartment. The degradation of amyloplasts and the reduction in starch granule size in taproot related to aging is in line with the transfer of carbon to reproductive organs (Rossato *et al.*, 2001, 2002a). A decrease of starch concentration is thus a valuable marker of the progress of senescence in rapeseed taproot, which coincides with the decrease of root biomass.

Electron microscopy revealed ferritin deposition at T1 in the amyloplasts of taproot regardless of nitrate conditions. Ferritin deposition was even higher at T2 (Venzhik *et al.*, 2019), consistent with the accumulation of iron between T1 and T2 (Fig. 4; Supplementary Fig. S1). The proteomic data presented above confirmed the higher abundance of ferritin proteins in the taproot of LN plants [ferritin 1 (XP_013723422.1), 3 (XP_013648011.1, XP_022547543.1), and 4 (XP_013687876.1); Supplementary Table S13]. The overaccumulation of iron with taproot aging could explain the overproduction of reactive oxygen species leading to taproot browning. Iron sequestration by ferritin seems to avoid the production of OH· radicals by the Fenton reaction (Deák *et al.*, 1999). Fe acts as a catalyst and must be avoided to prevent significant oxidative stress during senescence. The degradation of amyloplasts, which has already been reported in non-greening senescent cells (Inada *et al.*, 2000), and the accumulation of ferritin, which is considered a senescence marker in animal

(Wiley and Campisi, 2021) and plant (Murgia *et al.*, 2007) cells, indicate that the taproot undergoes senescence from T1 and that T2 corresponds to the late senescence stage.

Root proteins are nitrogen sources to sustain shoot growth and reproduction

Under HN, protein, amino acid, and total nitrogen contents fluctuate in parallel with aging in both the taproot and lateral roots (Fig. 5). They increase from T0 to T1, reflecting nitrogen storage in the root compartments, and decrease from T1 to T2, reflecting the remobilization of nitrogen to the shoot. Under LN, changes in total nitrogen, proteins, and amino acids with aging were different in taproot and lateral roots. Decreases in amino acids and proteins between T0 and T2 were only observed in taproot, while there was no significant decrease in the lateral roots (Rossato *et al.*, 2002b; Tilsner *et al.*, 2005). These results highlight the importance of the taproot as a nitrogen source. Protein decrease with ageing was consistent with the strong increase in protease activities with aging in the taproot under both LN and HN, and in the lateral roots when remobilization was enhanced by nitrate deficiency under LN.

Proteomic analysis reveals new senescence feature and molecular markers specific or common to taproot and lateral roots

The proteomic analyses performed in this study highlighted the main effects of aging on the physiology of taproot and lateral roots, identified new molecular markers for root senescence, and allowed us to compare leaf and root senescence markers.

Specific changes in taproot with aging are (i) the disappearance of protein categories related to nucleotide synthesis, translation, unfolded protein response (UPR) machinery that mitigates endoplasmic reticulum (ER) stress, and response to carbohydrates; and (ii) the appearance of protein categories related to amino acid catabolism, protein quality control, and cell wall catabolism.

Specific changes in lateral roots with aging are (i) the disappearance of protein categories related to anabolism, synthesis of fatty acids, amino acids and organic acids, and sulfate assimilation; and (ii) the appearance of processes related to the disorganization of protein complexes, cytoskeletons, actin filaments, and alternative respiration pentose phosphate-related NADH production. The common features exacerbated during the taproot and lateral root early development are associated with DNA replication, translation, redox control, pyridine metabolism, ribosome assembly, Ehrlich amino acid catabolism for the formation of aldehydes and alcohol, and flavonoid synthesis. Protein categories common to the taproot and lateral root senescence include functions related to the degradation of hydrogen peroxide, detoxification, respiration, and pentose metabolism. Thus, overall, the categories specific or common to the young taproot and lateral root organs are mostly related to anabolic functions, neosynthesis of metabolites, cell growth, and maintenance involving DNA replication and translation. The senescence categories specific or common to taproot and lateral roots are mostly related to the catabolism of proteins, amino acids, and cell wall, to detoxification, and to alternative energy metabolism. This comprehensive picture of root senescence thus shows many common features with the leaf senescence events reported by many studies (Guo and Gan, 2005; Breeze *et al.*, 2011) with the exception of the aspects related to chloroplast degradation.

As is the case during leaf senescence, many proteases were modified with root senescence, and several proteases were revealed as good root senescence markers (Fig. 10; Buchanan-Wollaston and Ainsworth, 1996; Guo *et al.*, 2004; Martínez *et al.*, 2007; Roberts *et al.*, 2012; Girondé *et al.*, 2016; Poret *et al.*, 2016). In taproot and lateral roots, the senescence-induced proteases were mainly cysteine, serine, and aspartate proteases, while the senescence-repressed proteases belong to the proteasome and metallo-protease class (Fig. 10; Supplementary Fig. S4). The increase of cysteine proteases in senescing roots is consistent with the decrease of cysteine protease inhibitors (Fig. 11). Cysteine proteases have been described as the prominent protease class of senescing leaves (Buchanan-Wollaston and Ainsworth, 1996; Guo *et al.*, 2004; Martínez *et al.*, 2007; Roberts *et al.*, 2012; Girondé *et al.*, 2016; Poret *et al.*, 2016). Papain-like cysteine proteases (PLCPs) promote massive protein degradation during leaf senescence (Parrott *et al.*, 2010), and the SAG2 and SAG12 PLCPs are well-known leaf senescence markers (Hensel *et al.*, 1993; Noh and Amasino, 1999; Gombert *et al.*, 2006). Notably, the RD21A, RD21B, RD21C, RD19A, RD19C, Cathepsin B3, and SAG12 PLCPs are common senescence markers of taproot and leaves in both rapeseed and Arabidopsis leaves (Noh and Amasino, 1999; Poret *et al.*, 2016; Pružinská *et al.*, 2017).

While the overall protease activities were lower in the taproot than in the lateral roots (Fig. 6), it was surprising to see that the diversity of the proteases of the taproot was higher than in the lateral roots. We hypothesized that the taproot-specific proteases could be more specific for the degradation of the protein reserves and possibly of the cell wall. Indeed, senescence-associated proteases in the taproot were mainly serine carboxypeptidases such as SCPL7 (XP_013672786.1), SCPL28 (XP_013659509.1), SCPL29 (XP_013720411.1), and SCPL50 (XP_013674515.1), which are known to be extracellular. Their involvement in senescence-associated cell wall modifications could explain the decrease in cell cohesion in taproots with aging. An increase in serine carboxypeptidases has been reported in senescing leaves by Borniego *et al.* (2020), and probably played a role in programmed cell death in the leaves of *Avena sativa* (Coffeen and Wolpert, 2004). The specific accumulation of several Clp proteases (ClpR1, XP_013735849.1; ClpR2, XP_013698293.1; ClpR4, XP_013671352.1; Clp4, XP_013670730.1; and Clp6, XP_013657456.1) in taproot was also observed. These proteins are involved in chloroplast degradation during leaf senescence (Roberts *et al.*, 2002; Kato and Sakamoto, 2010; Diaz-Mendoza *et al.*, 2016). Their increase in

taproot with aging suggests that they could be involved in the degradation of amyloplasts (Fig. 4).

Common and specific protein markers can be identified for leaf, lateral root, and taproot senescence

The exploration of the transcriptomic data from Breeze *et al.* (2011) and transcriptomic data from Tamary *et al.* (2019) led us to shortlist markers that are shared between leaf senescence and root senescence in *Brassicaceae*. These markers, including SDPs and SAPs, will facilitate further studies on root senescence (Supplementary Table S7). Such a comparison revealed that the management of carbohydrate and nucleobase catabolism is a common feature of root and leaf senescence. The catabolism of nucleobases, and especially of purine, could increase the pool of remobilizable nitrogen in both organs. Their degradation products (glyoxylate and ammonia) could indeed be an important source of nitrogen for the reproductive parts (Brychkova *et al.*, 2008a, b; Werner and Witte, 2011). In contrast to nitrogen metabolism, including amino acid catabolism, that has been largely studied in senescing leaves, the catabolism of nucleobases and its role in nutrient remobilization has been poorly investigated so far (Hildebrandt *et al.*, 2015; Havé *et al.*, 2017).

Conclusion

For the first time, this work provides an integrative view of the metabolic changes occurring during the senescence of the taproot and lateral roots of rapeseed. It has led to the identification of many new molecular players (including proteases) involved in this process, some of which are specific to roots while others are common to leaf senescence. Thus, root senescence requires specific catabolic pathways (such as nucleic acid degradation) that have not been considered much until now and deserve particular attention to better understand nutrient remobilization from roots. Finally, this study also provides a novel set of molecular markers available to assess more accurately the progression of root senescence.

Supplementary data

The following supplementary data are available at *JXB* online.

Fig. S1. Iron concentration in taproot during the development of rapeseed cultivated under high or low nitrogen conditions.

Fig. S2. Clustering of the proteases modulated in the taproot and lateral root tissues during the development of rapeseed cultivated under low nitrogen conditions.

Fig. S3. Starch content in lateral roots during the development of rapeseed cultivated under high or low nitrogen conditions.

Fig. S4. Proteases with significantly increased accumulation between beginning of flowering and pod development stages in taproot and lateral roots of rapeseed cultivated under low nitrogen conditions.

Table S1. Identification and XIC-based quantification of proteins in the taproot under low nitrogen conditions.

Table S2. Identification and spectral count quantification of proteins in the taproot under low nitrogen conditions.

Table S3. Identification and XIC-based quantification of proteins in the lateral roots under low nitrogen conditions.

Table S4. Identification and spectral count quantification of proteins in the lateral roots under low nitrogen conditions.

Table S5. Identification of proteins in the taproot under low nitrogen condition in each cluster of the heatmap (Fig. 7A).

Table S6. Identification of proteins in the lateral roots under low nitrogen condition in each cluster of the heatmap (Fig. 7B).

Table S7 Identification of proteins belonging to the different marker clusters identified in taproot and lateral root (Fig. 9A) under low nitrogen condition.

Table S8. Biological process enrichment in the taproot under low nitrogen conditions.

Table S9. Biological process enrichment in the lateral roots under low nitrogen conditions.

Table S10. Biological process enrichment of different clusters and their intersection under low nitrogen conditions.

Table S11. Identification of proteases in the taproot under low nitrogen conditions in each cluster of the heatmap (Fig. 8C).

Table S12. Identification of proteases in the lateral roots under low nitrogen conditions in each cluster of the heatmap (Fig. 8C).

Table S13. Abundance of proteins related to iron storage identified in the taproot under low nitrogen conditions.

Protocol S1. Chromatographic and mass spectrometry parameters.

Protocol S2. Protein identification parameters.

Acknowledgements

We are most grateful to the PLATIN (Plateau d'Isotopie de Normandie) core facility for elemental analysis, Dr Didier Goux from the CMABIO[3] platform for the microscopy analyses, Dr Benoît Bernay from the Proteogen platform for his help to proteomic analysis, Julie Frémont for her technical assistance, and Dr Adrian Dauphine for proofreading and English editing.

Author contributions

MJ, PE, and JT: conceptualization; MJ and TB: investigation; MJ and TB: data curation; MJ: formal analysis; MJ, PE, JT, and CMD: visualization; MJ, PE, JT, and CMD: writing—original draft preparation; AM, FC, TB, CMD, PE, and JT: writing—review & editing; CMD, PE, and JT: supervision; CMD, and PE: funding acquisition.

Conflict of interest

The authors declare that the research was conducted in the absence of any commercial or financial relationships that could be construed as a potential conflict of interest.

Funding

This work was supported by the French National Research Agency (ANR-19-CE14-0009-02 hAPPEN: Autophagy, Proteases and plant Performances). The IJPB benefits from the support of Saclay Plant Sciences-SPS (ANR-17-EUR-0007).

Data availability

The mass spectrometry proteomics data are available in the ProteomeXchange Consortium via the PRIDE (Perez-Riverol *et al.*, 2022) partner repository with the dataset identifier PXD050894.

References

Avice J-C, Etienne P. 2014. Leaf senescence and nitrogen remobilization efficiency in oilseed rape (*Brassica napus* L.). Journal of Experimental Botany **65**, 3813–3824.

Baldi E, Wells CE, Marangoni B. 2010. Nitrogen absorption and respiration in white and brown peach roots. Journal of Plant Nutrition **33**, 461–469.

Balliau T, Blein-Nicolas M, Zivy M. 2018. Evaluation of optimized tube-gel methods of sample preparation for large-scale plant proteomics. Proteomes **6**, 6.

Belouah I, Bénard C, Denton A, *et al*. 2020. Transcriptomic and proteomic data in developing tomato fruit. Data in Brief **28**, 105015.

Bindea G, Mlecnik B, Hackl H, Charoentong P, Tosolini M, Kirilovsky A, Fridman W-H, Pagès F, Trajanoski Z, Galon J. 2009. ClueGO: a Cytoscape plug-in to decipher functionally grouped gene ontology and pathway annotation networks. Bioinformatics **25**, 1091–1093.

Bingham IJ. 2007. Quantifying the presence and absence of turgor for the spatial characterization of cortical senescence in roots of *Triticum aestivum* (Poaceae). American Journal of Botany **94**, 2054–2058.

Borniego ML, Molina MC, Guiamét JJ, Martinez DE. 2020. Physiological and proteomic changes in the apoplast accompany leaf senescence in Arabidopsis. Frontiers in Plant Science **10**, 1635.

Bradford MM. 1976. A rapid and sensitive method for the quantitation of microgram quantities of protein utilizing the principle of protein–dye binding. Analytical Biochemistry **72**, 248–254.

Breeze E, Harrison E, McHattie S, *et al*. 2011. High-resolution temporal profiling of transcripts during Arabidopsis leaf senescence reveals a distinct chronology of processes and regulation. The Plant Cell **23**, 873–894.

Brychkova G, Alikulov Z, Fluhr R, Sagi M. 2008a. A critical role for ureides in dark and senescence-induced purine remobilization is unmasked in the *Atxdh1* Arabidopsis mutant. The Plant Journal **54**, 496–509.

Brychkova G, Fluhr R, Sagi M. 2008b. Formation of xanthine and the use of purine metabolites as a nitrogen source in Arabidopsis plants. Plant Signaling & Behavior **3**, 999–1001.

Buchanan-Wollaston V. 1997. The molecular biology of leaf senescence. Journal of Experimental Botany **48**, 181–199.

Buchanan-Wollaston V, Ainsworth C. 1996. Leaf senescence in *Brassica napus*: cloning of senescence related genes by subtractive hybridisation. Plant Molecular Biology **33**, 821–834.

Cao J, Liu H, Tan S, Li Z. 2023. Transcription factors-regulated leaf senescence: current knowledge, challenges and approaches. International Journal of Molecular Sciences **24**, 9245.

Coffeen WC, Wolpert TJ. 2004. Purification and characterization of serine proteases that exhibit caspase-like activity and are associated with programmed cell death in *Avena sativa*. The Plant Cell **16**, 857–873.

Comas LH, Eissenstat DM, Lakso AN. 2000. Assessing root death and root system dynamics in a study of grape canopy pruning. New Phytologist **147**, 171–178.

Deák M, Horváth GV, Davletova S, Török K, Sass L, Vass I, Barna B, Király Z, Dudits D. 1999. Plants ectopically expressing the ironbinding protein, ferritin, are tolerant to oxidative damage and pathogens. Nature Biotechnology **17**, 192–196.

Desclos M, Etienne P, Coquet L, Jouenne T, Bonnefoy J, Segura R, Reze S, Ourry A, Avice J-C. 2009. A combined 15N tracing/proteomics study in *Brassica napus* reveals the chronology of proteomics events associated with N remobilisation during leaf senescence induced by nitrate limitation or starvation. Proteomics **9**, 3580–3608.

Diaz-Mendoza M, Velasco-Arroyo B, Santamaria ME, González-Melendi P, Martinez M, Diaz I. 2016. Plant senescence and proteolysis: two processes with one destiny. Genetics and Molecular Biology **39**, 329–338.

Edgar R, Domrachev M, Lash AE. 2002. Gene expression omnibus: NCBI gene expression and hybridization array data repository. Nucleic Acids Research **30**, 207–210.

Eissenstat D. 2000. Root structure and function in an ecological context. New Phytologist **148**, 353–354.

Girondé A, Etienne P, Trouverie J, *et al*. 2015. The contrasting N management of two oilseed rape genotypes reveals the mechanisms of proteolysis associated with leaf N remobilization and the respective contributions of leaves and stems to N storage and remobilization during seed filling. BMC Plant Biology **15**, 59.

Girondé A, Poret M, Etienne P, Trouverie J, Bouchereau A, Le Cahérec F, Leport L, Niogret M-F, Avice J-C. 2016. A comparative study of proteolytic mechanisms during leaf senescence of four genotypes of winter oilseed rape highlighted relevant physiological and molecular traits for NRE improvement. Plants **5**, 1.

Gombert J, Dily FL, Lothier J, Etienne P, Rossato L, Allirand J-M, Jullien A, Savin A, Ourry A. 2010. Effect of nitrogen fertilization on nitrogen dynamics in oilseed rape using ^{15}N-labeling field experiment. Journal of Plant Nutrition and Soil Science **173**, 875–884.

Gombert J, Etienne P, Ourry A, Dily FL. 2006. The expression patterns of SAG12/Cab genes reveal the spatial and temporal progression of leaf senescence in *Brassica napus* L. with sensitivity to the environment. Journal of Experimental Botany **57**, 1949–1956.

Gregersen PL, Culetic A, Boschian L, Krupinska K. 2013. Plant senescence and crop productivity. Plant Molecular Biology **82**, 603–622.

Guo Y, Cai Z, Gan S. 2004. Transcriptome of Arabidopsis leaf senescence. Plant, Cell & Environment **27**, 521–549.

Guo Y, Gan S. 2005. Leaf senescence: signals, execution, and regulation. Current Topics in Developmental Biology **71**, 83–112.

Havé M, Marmagne A, Chardon F, Masclaux-Daubresse C. 2017. Nitrogen remobilization during leaf senescence: lessons from Arabidopsis to crops. Journal of Experimental Botany **68**, 2513–2529.

Henry CM, Deacon JW. 1981. Natural (non-pathogenic) death of the cortex of wheat and barley seminal roots, as evidenced by nuclear staining with acridine orange. Plant and Soil **60**, 255–274.

Hensel LL, Grbić V, Baumgarten DA, Bleecker AB. 1993. Developmental and age-related processes that influence the longevity and senescence of photosynthetic tissues in arabidopsis. The Plant Cell **5**, 553–564.

Hildebrandt TM, Nunes Nesi A, Araújo WL, Braun H-P. 2015. Amino acid catabolism in plants. Molecular Plant **8**, 1563–1579.

Inada N, Sakai A, Kuroiwa H, Kuroiwa T. 2000. Senescence in the nongreening region of the rice (*Oryza sativa*) coleoptile. Protoplasma **214**, 180–193.

James M, Masclaux-Daubresse C, Marmagne A, Azzopardi M, Laîné P, Goux D, Etienne P, Trouverie J. 2019. A new role for SAG12 cysteine protease in roots of *Arabidopsis thaliana*. Frontiers in Plant Science **9**, 1998.

James M, Poret M, Masclaux-Daubresse C, Marmagne A, Coquet L, Jouenne T, Chan P, Trouverie J, Etienne P. 2018. SAG12, a major cysteine protease involved in nitrogen allocation during senescence for seed production in *Arabidopsis thaliana*. Plant and Cell Physiology **59**, 2052–2063.

Katari MS, Nowicki SD, Aceituno FF, *et al*. 2010. VirtualPlant: a software platform to support systems biology research. Plant Physiology **152**, 500–515.

Kato Y, Sakamoto W. 2010. New insights into the types and function of proteases in plastids. International Review of Cell and Molecular Biology **280**, 185–218.

Kohli A, Narciso JO, Miro B, Raorane M. 2012. Root proteases: reinforced links between nitrogen uptake and mobilization and drought tolerance. Physiologia Plantarum **145**, 165–179.

Langella O, Valot B, Balliau T, Blein-Nicolas M, Bonhomme L, Zivy M. 2017. X!TandemPipeline: a tool to manage sequence redundancy for protein inference and phosphosite identification. Journal of Proteome Research **16**, 494–503.

Lee S, Masclaux-Daubresse C. 2021. Current understanding of leaf senescence in rice. International Journal of Molecular Sciences **22**, 4515.

Liu Z, Marella CBN, Hartmann A, Hajirezaei MR, von Wirén N. 2019. An age-dependent sequence of physiological processes defines developmental root senescence. Plant Physiology **181**, 993–1007.

Lynch JP. 2019. Root phenotypes for improved nutrient capture: an underexploited opportunity for global agriculture. New Phytologist **223**, 548–564.

MacLeod W, Robson AD, Abbott LK. 1986. Effects of phosphate supply and inoculation with a vesicular-arbuscular mycorrhizal fungus on the death of the root cortex of wheat, rape and subterranean clover. New Phytologist **103**, 349–357.

Maillard A, Etienne P, Diquélou S, Trouverie J, Billard V, Yvin J-C, Ourry A. 2016. Nutrient deficiencies modify the ionomic composition of plant tissues: a focus on cross-talk between molybdenum and other nutrients in *Brassica napus*. Journal of Experimental Botany **67**, 5631–5641.

Malagoli P, Laine P, Rossato L, Ourry A. 2005. Dynamics of nitrogen uptake and mobilization in field-grown winter oilseed rape (*Brassica napus*) from stem extension to harvest: I. Global N flows between vegetative and reproductive tissues in relation to leaf fall and their residual N. Annals of Botany **95**, 853–861.

Martínez DE, Bartoli CG, Grbic V, Guiamet JJ. 2007. Vacuolar cysteine proteases of wheat (*Triticum aestivum* L.) are common to leaf senescence induced by different factors. Journal of Experimental Botany **58**, 1099–1107.

Masclaux C, Valadier M-H, Brugière N, Morot-Gaudry J-F, Hirel B. 2000. Characterization of the sink/source transition in tobacco (*Nicotiana tabacum* L.) shoots in relation to nitrogen management and leaf senescence. Planta **211**, 510–518.

McIlvaine TC. 1921. A buffer solution for colorimetric comparaison. Journal of Biological Chemistry **49**, 183–186.

Mi H, Muruganujan A, Huang X, Ebert D, Mills C, Guo X, Thomas PD. 2019. Protocol update for large-scale genome and gene function analysis with the PANTHER classification system (v.14.0). Nature Protocols **14**, 703–721.

Murgia I, Vazzola V, Tarantino D, Cellier F, Ravet K, Briat J-F, Soave C. 2007. Knock-out of ferritin AtFer1 causes earlier onset of age-dependent leaf senescence in Arabidopsis. Plant Physiology and Biochemistry **45**, 898–907.

Noh YS, Amasino RM. 1999. Regulation of developmental senescence is conserved between Arabidopsis and *Brassica napus*. Plant Molecular Biology **41**, 195–206.

Paramonova NV, Shevyakova NI, Kuznetsov VV. 2007. Ultrastructure of ferritin in the leaves of *Mesembryanthemum crystallinum* under stress conditions. Russian Journal of Plant Physiology **54**, 244–256.

Parrott DL, Martin JM, Fischer AM. 2010. Analysis of barley (*Hordeum vulgare*) leaf senescence and protease gene expression: a family C1A cysteine protease is specifically induced under conditions characterized by high carbohydrate, but low to moderate nitrogen levels. New Phytologist **187**, 313–331.

Perez-Riverol Y, Bai J, Bandla C, *et al*. 2022. The PRIDE database resources in 2022: a hub for mass spectrometry-based proteomics evidences. Nucleic Acids Research **50**, D543–D552.

Poret M, Chandrasekar B, van der Hoorn RAL, Avice J-C. 2016. Characterization of senescence-associated protease activities involved in the efficient protein remobilization during leaf senescence of winter oilseed rape. Plant Science **246**, 139–153.

Poret M, Chandrasekar B, van der Hoorn RAL, Déchaumet S, Bouchereau A, Kim T-H, Lee B-R, Macquart F, Hara-Nishimura I, Avice J-C. 2019. A genotypic comparison reveals that the improvement in nitrogen remobilization efficiency in oilseed rape leaves is related to specific patterns of senescence-associated protease activities and phytohormones. Frontiers in Plant Science **10**, 46.

Pružinská A, Shindo T, Niessen S, Kaschani F, Tóth R, Millar AH, van der Hoorn RAL. 2017. Major Cys protease activities are not essential for senescence in individually darkened Arabidopsis leaves. BMC Plant Biology **17**, 4.

Roberts I, Murray PF, Passeron S, Barneix AJ. 2002. The activity of the 20S proteasome is maintained in detached wheat leaves during senescence in darkness. Plant Physiology and Biochemistry **40**, 161–166.

Roberts IN, Caputo C, Criado MV, Funk C. 2012. Senescence-associated proteases in plants. Physiologia Plantarum **145**, 130–139.

Rossato L, Lainé P, Ourry A. 2001. Nitrogen storage and remobilization in *Brassica napus* L. during the growth cycle: nitrogen fluxes within the plant and changes in soluble protein patterns. Journal of Experimental Botany **52**, 1655–1663.

Rossato L, Le Dantec C, Laine P, Ourry A. 2002a. Nitrogen storage and remobilization in *Brassica napus* L. during the growth cycle: identification, characterization and immunolocalization of a putative taproot storage glycoprotein. Journal of Experimental Botany **53**, 265–275.

Rossato L, MacDuff JH, Laine P, Le Deunff E, Ourry A. 2002b. Nitrogen storage and remobilization in *Brassica napus* L. during the growth cycle: effects of methyl jasmonate on nitrate uptake, senescence, growth, and VSP accumulation. Journal of Experimental Botany **53**, 1131–1141.

Schneider HM, Lynch JP. 2018. Functional implications of root cortical senescence for soil resource capture. Plant and Soil **423**, 13–26.

Schneider HM, Wojciechowski T, Postma JA, Brown KM, Lücke A, Zeisler V, Schreiber L, Lynch JP. 2017. Root cortical senescence decreases root respiration, nutrient content and radial water and nutrient transport in barley. Plant, Cell & Environment **40**, 1392–1408.

Tamary E, Nevo R, Naveh L, Levin-Zaidman S, Kiss V, Savidor A, Levin Y, Eyal Y, Reich Z, Adam Z. 2019. Chlorophyll catabolism precedes changes in chloroplast structure and proteome during leaf senescence. Plant Direct **3**, e00127.

Tilsner J, Kassner N, Struck C, Lohaus G. 2005. Amino acid contents and transport in oilseed rape (*Brassica napus* L.) under different nitrogen conditions. Planta **221**, 328–338.

Valot B, Langella O, Nano E, Zivy M. 2011. MassChroQ: a versatile tool for mass spectrometry quantification. Proteomics **11**, 3572–3577.

Venzhik YV, Shchyogolev SY, Dykman LA. 2019. Ultrastructural reorganization of chloroplasts during plant adaptation to abiotic stress factors. Russian Journal of Plant Physiology **66**, 850–863.

Werner AK, Witte C-P. 2011. The biochemistry of nitrogen mobilization: purine ring catabolism. Trends in Plant Science **16**, 381–387.

Wiley CD, Campisi J. 2021. The metabolic roots of senescence: mechanisms and opportunities for intervention. Nature Metabolism **3**, 1290–1301.

Wojciechowska N, Sobieszczuk-Nowicka E, Bagniewska-Zadworna A. 2018. Plant organ senescence—regulation by manifold pathways. Plant Biology **20**, 167–181.

Wojciechowska N, Wilmowicz E, Marzec-Schmidt K, Ludwików A, Bagniewska-Zadworna A. 2020. Abscisic acid and jasmonate metabolisms are jointly regulated during senescence in roots and leaves of *Populus trichocarpa*. International Journal of Molecular Sciences **21**, 2042.

Zhu L, Liu L, Sun H, Zhang Y, Zhu J, Zhang K, Li A, Bai Z, Wang G, Li C. 2021. Physiological and comparative transcriptomic analysis provide insight into cotton (*Gossypium hirsutum* L.) root senescence in response. Frontiers in Plant Science **12**, 748715.